Role of Phase Domains in Complex Materials

Ian Robinson
University College London
Brookhaven National Laboratory

Tohoku Symposium
New Scientific Horizons with Synchrotron Radiation
Sendai, July 2026

Ferroelectric and Ferromagnetic Domains

G. Catalan, J. Seidel, R. Ramesh, J. F. Scott, RMP 84 119 (2012)

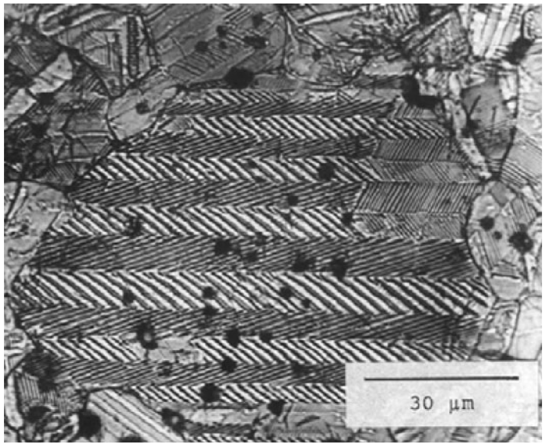

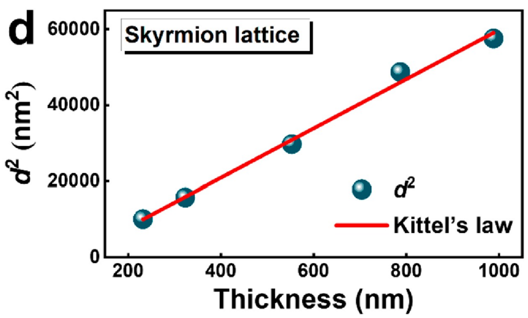

MFM Fe_3GaTe_2 thin films
S. Jin et al, Nano Lett. 24 5467 (2024)

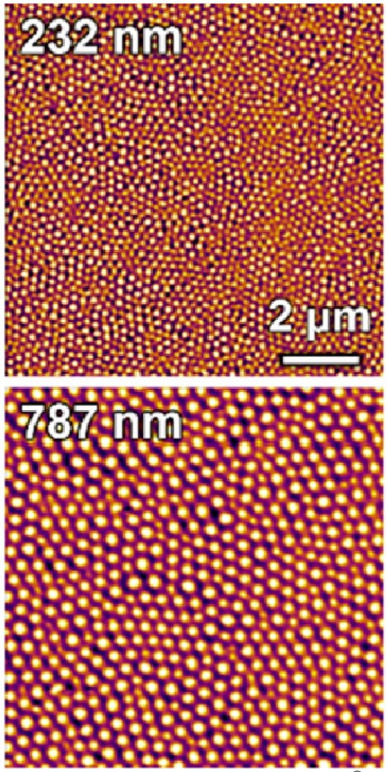

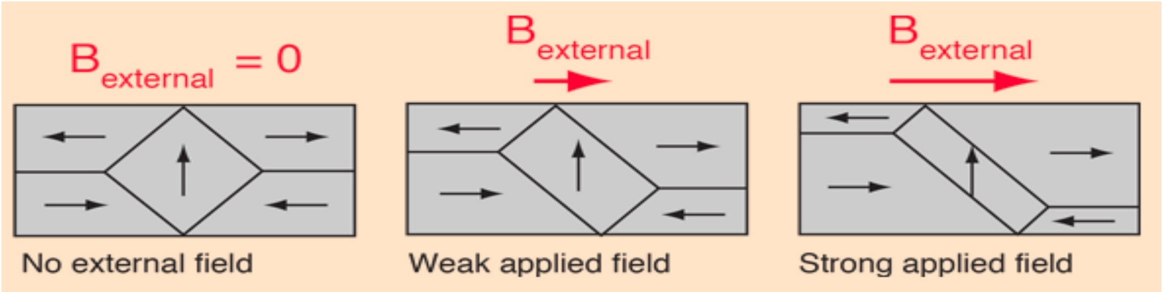

Stripe Domains in $PbTiO_3$ thin films

S. O. Hruszkewycz et al Phys. Rev. Lett. 110, 177601 (2013)

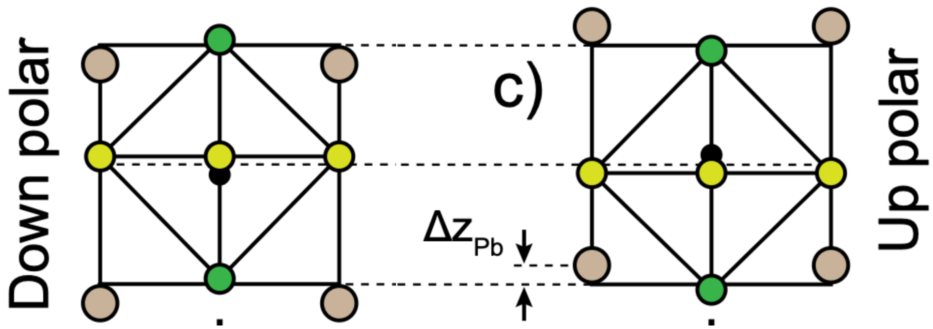

Phase of Structure Factor

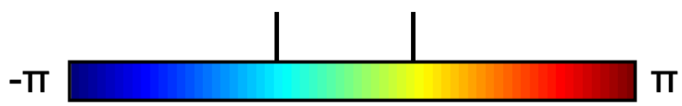

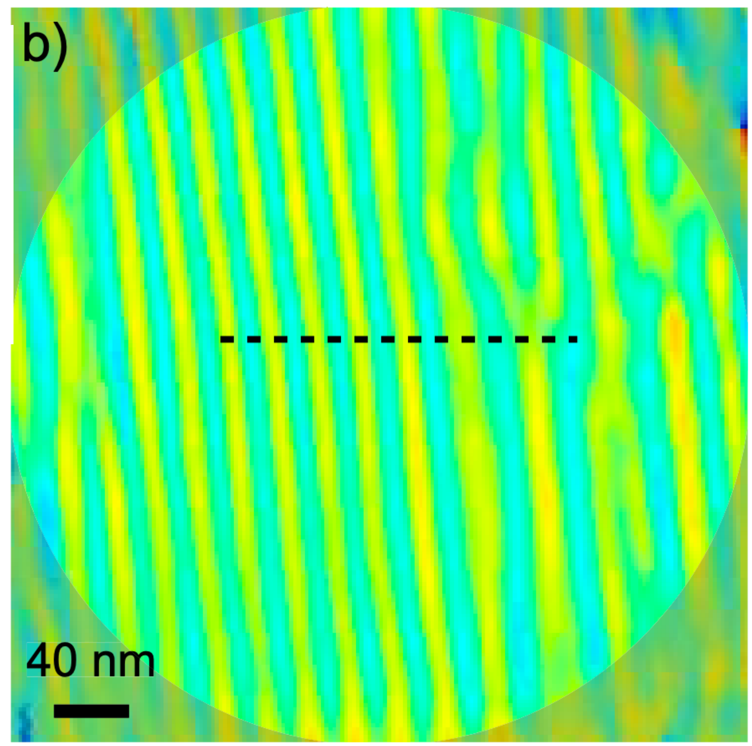

Geometric Phase Analysis (GPA) in TEM

M. J. Hÿtch et al, Nature **423** 270 (2003)

A. Lappas et al, Phys. Rev. X **9** 041044 (2019)

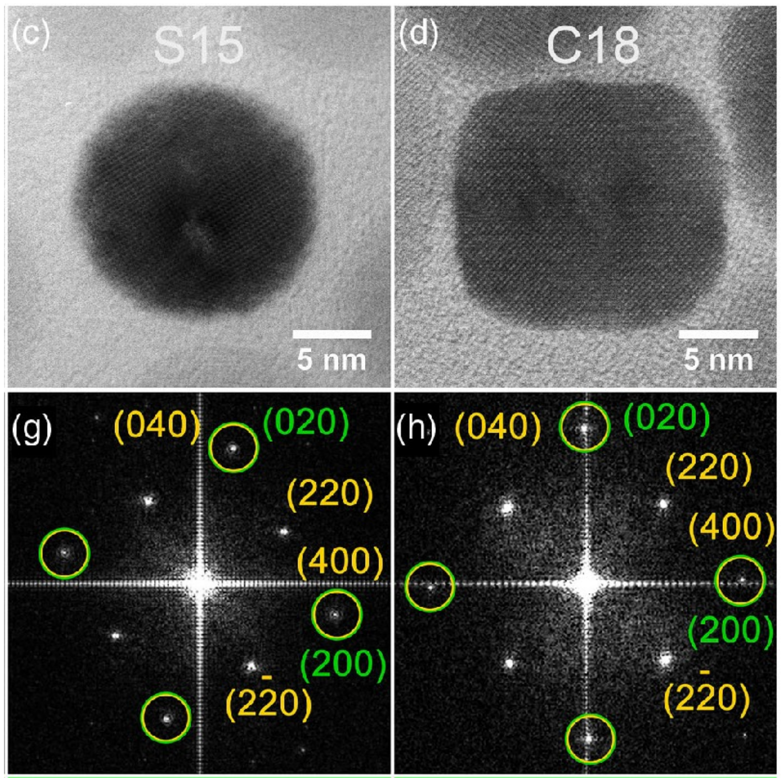

Fe_3O_4 nanoparticles

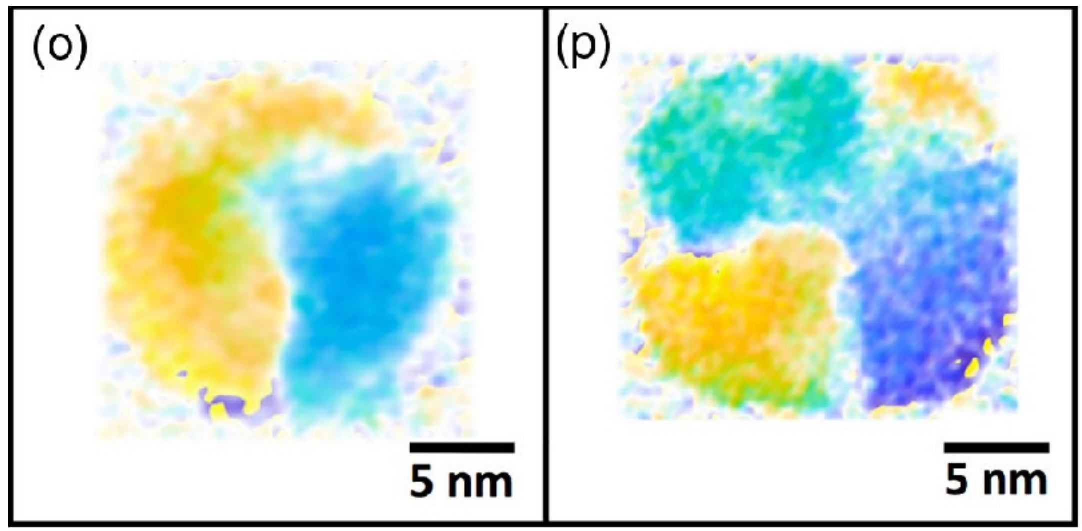

Coherent X-ray Diffraction Imaging

- Phase Domains in materials
- Coherent Diffraction Imaging (CDI)
- Bragg ptychography
- Spin-ordered domains in $La_{2-x}Sr_xNiO_4$
- $BaTiO_3$ in Multilayer Capacitors
- Domains in solid state electrolyte crystals
- Opportunities for CDI at NanoTerasu

(Resonant) Coherent X-ray Diffraction

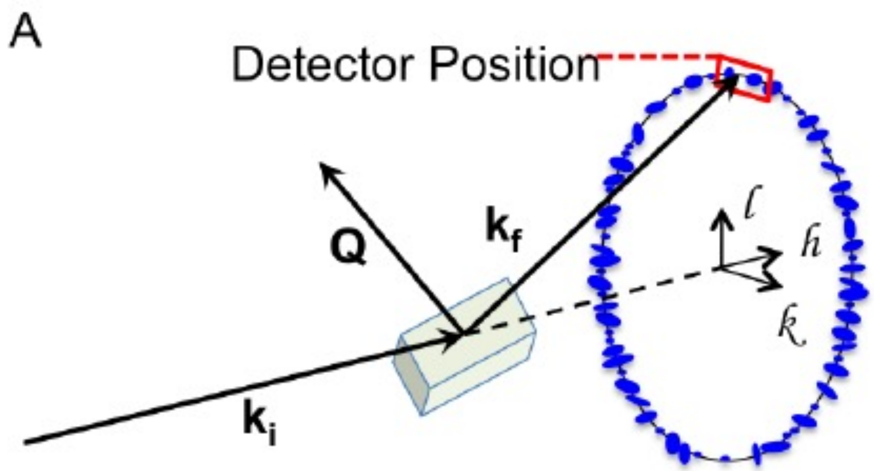

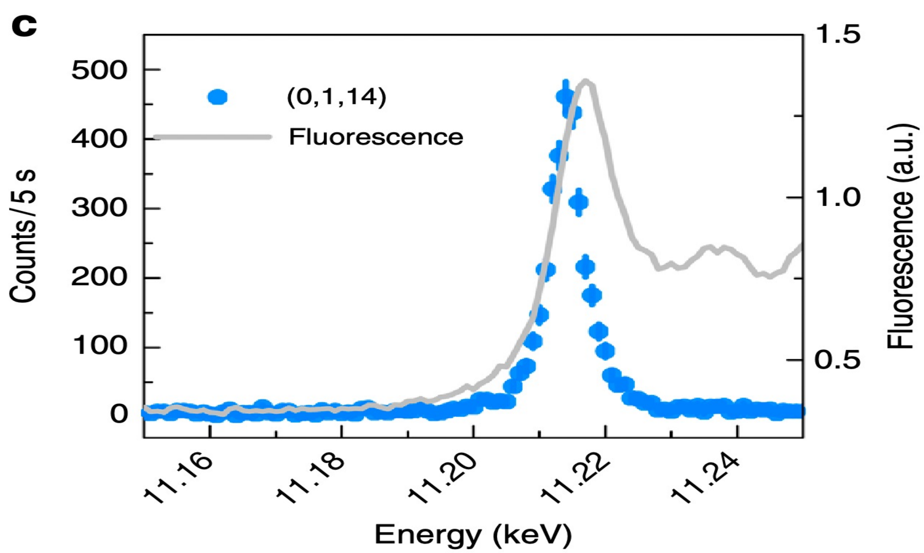

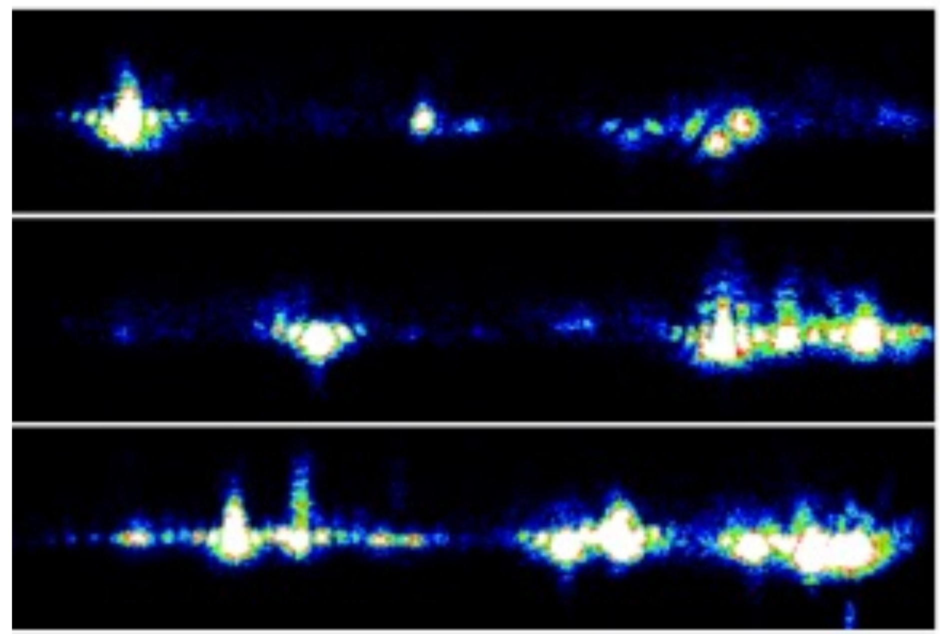

Generic "Error Reduction" method

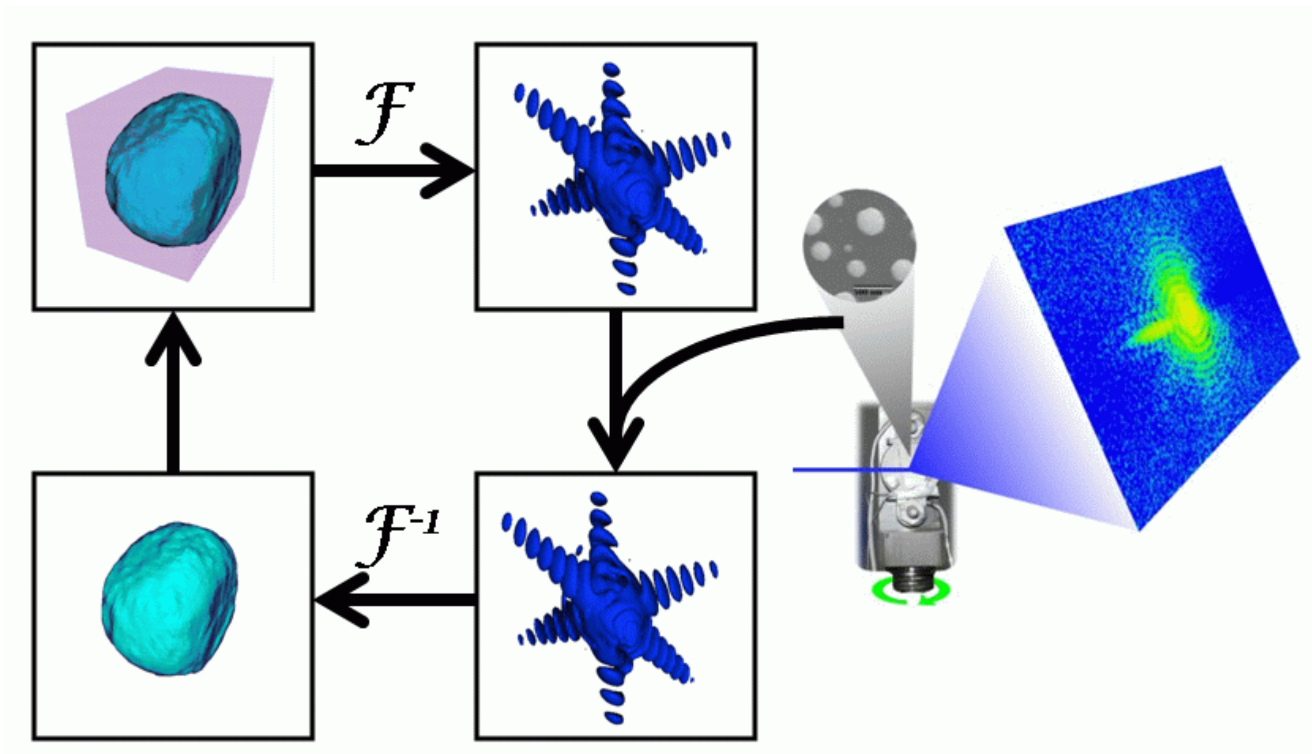

J. R. Fienup Appl. Opt. 21 2758 (1982)
R. W. Gerchberg and W. O. Saxton Optik 35 237 (1972)

Gold nanocrystal reconstruction

showing support used for 20 HIO followed by 10 ER

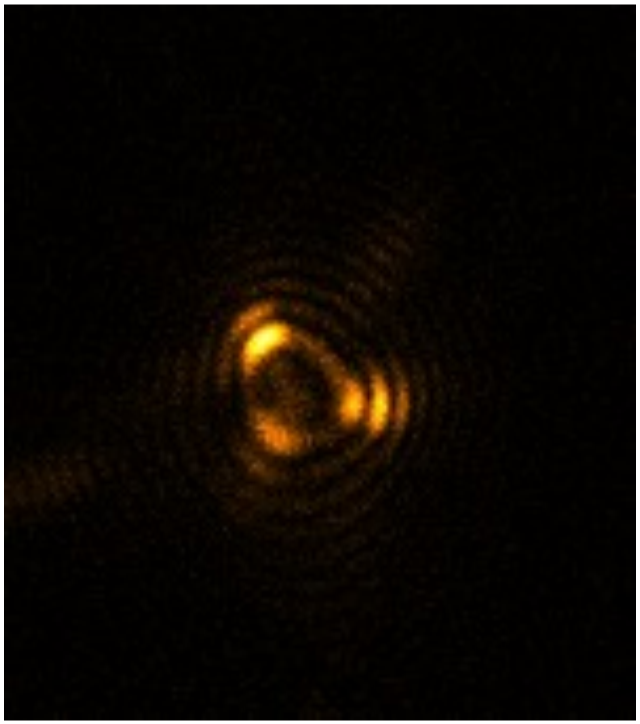

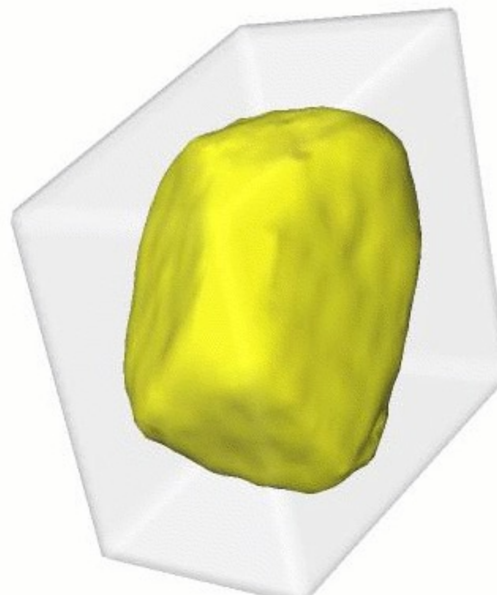

Phase isosurface showing residual strain

$$\Delta\phi = \mathbf{k}_f \cdot \mathbf{u} - \mathbf{k}_i \cdot \mathbf{u} = \mathbf{Q} \cdot \mathbf{u}$$

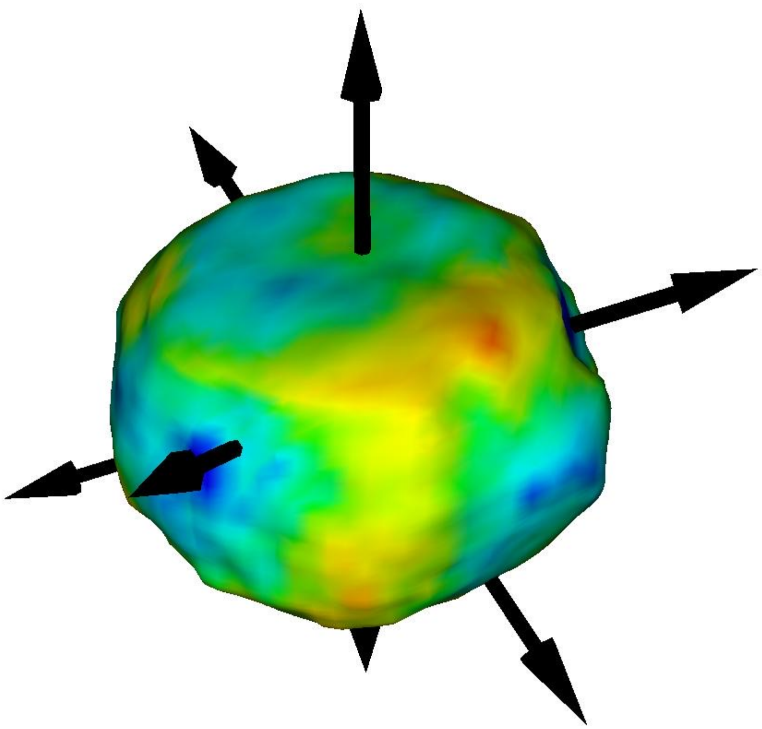

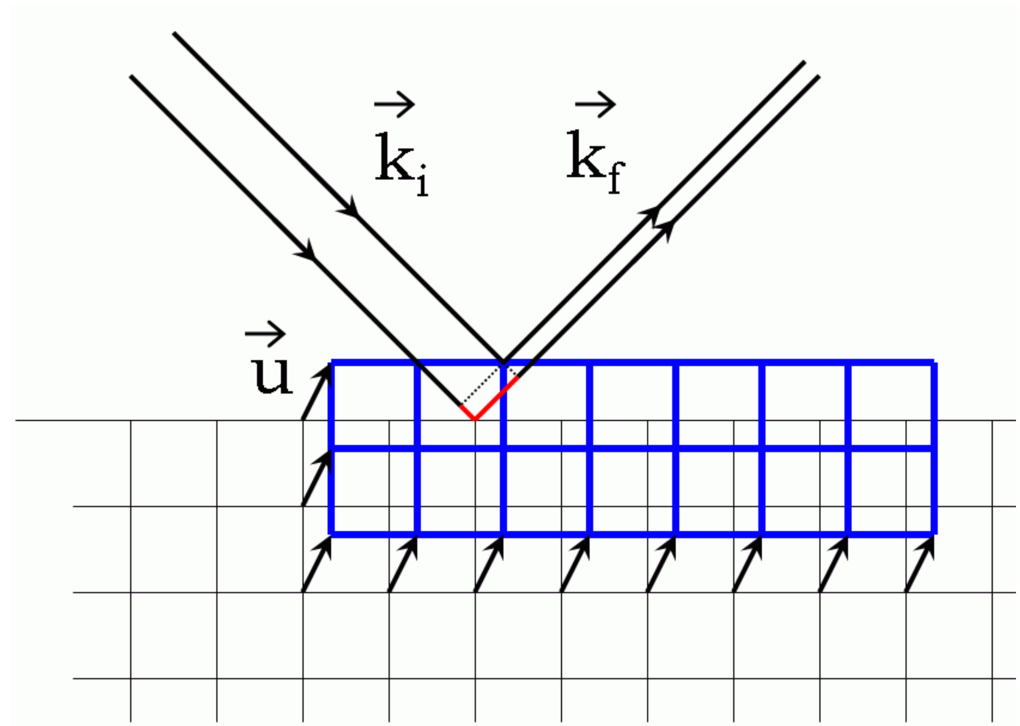

Sensitivity to domain offsets

$$\Delta\phi = \mathbf{k_f} \cdot \mathbf{u} - \mathbf{k_i} \cdot \mathbf{u} = \mathbf{Q} \cdot \mathbf{u}$$

Difficult convergence to unique solution

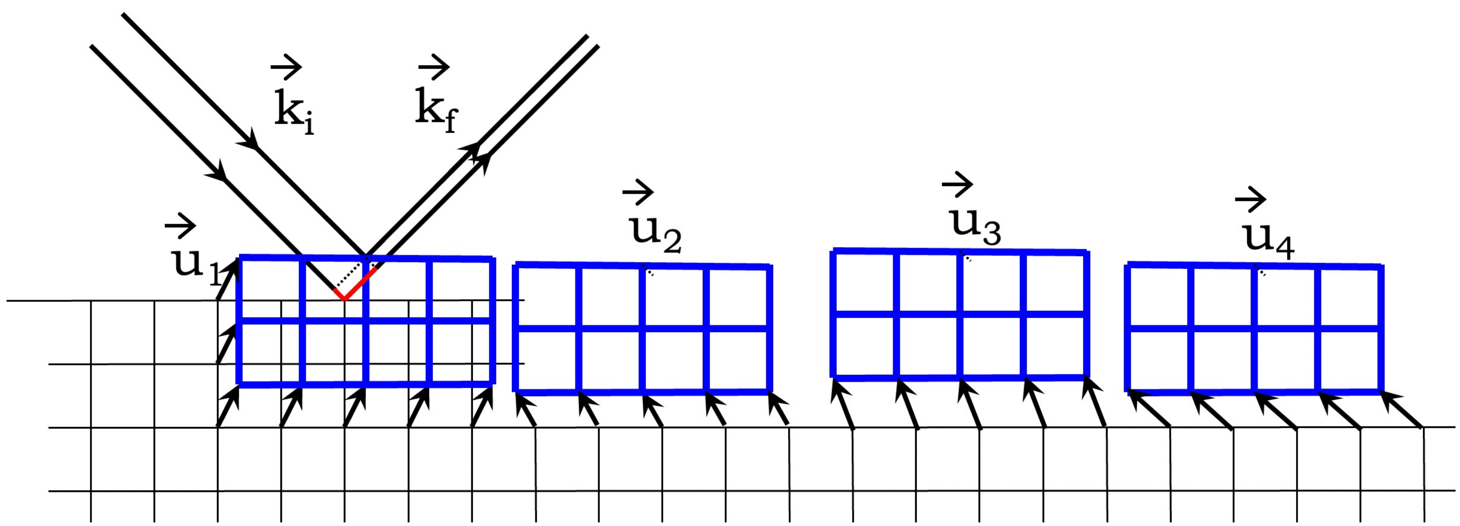

I. K. Robinson, Synchrotron Radiation News **37** 11 (2024)

X-ray Bragg Pytchography

J. Rodenburg et al, PRL 98, 034801 (2007)

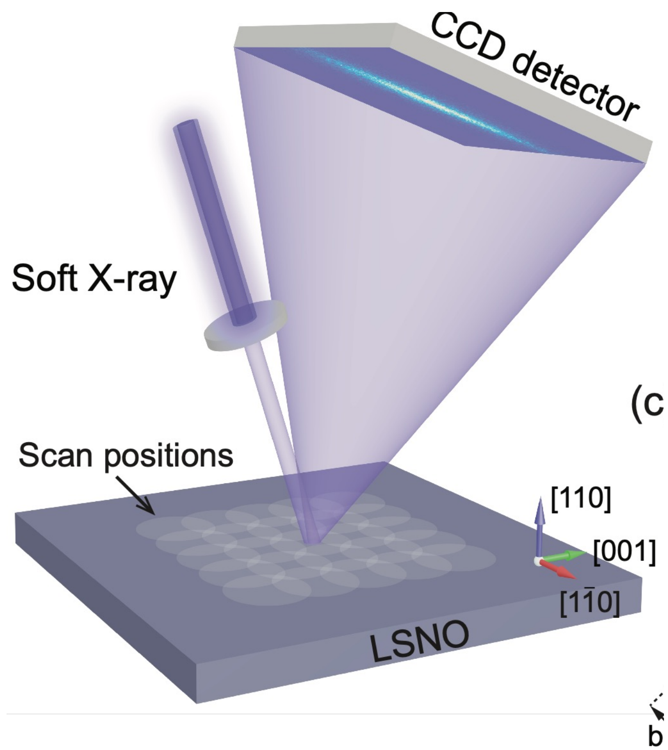

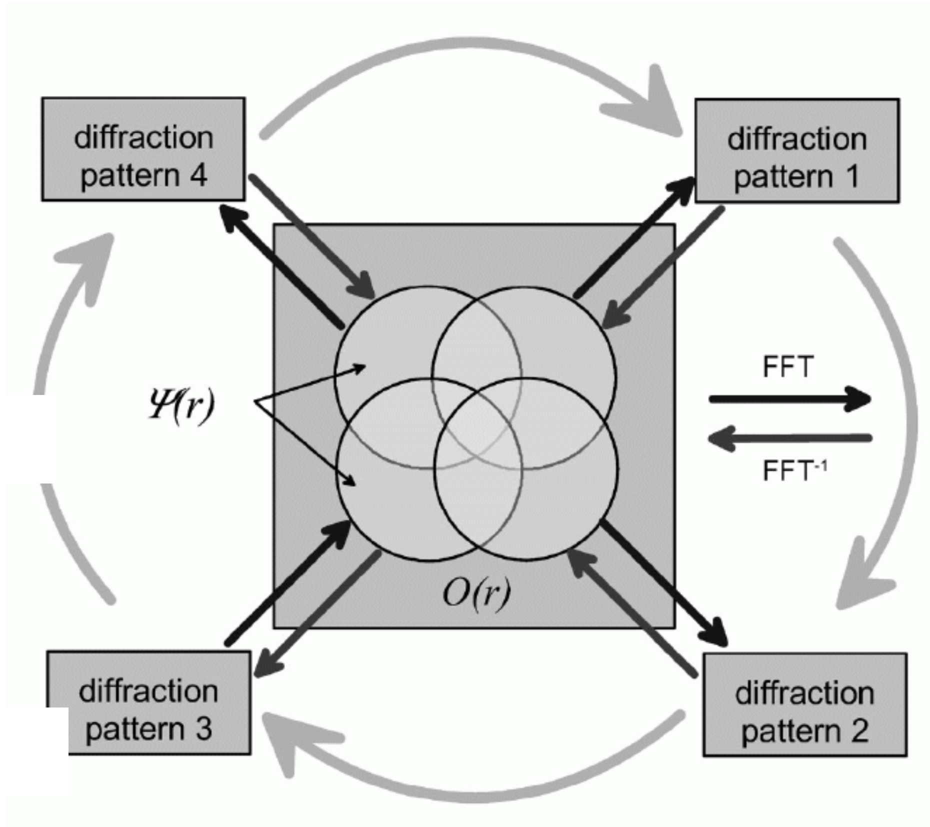

Phase Diagram $La_{2-x}Sr_xNiO_4$ is similar to Cuprates

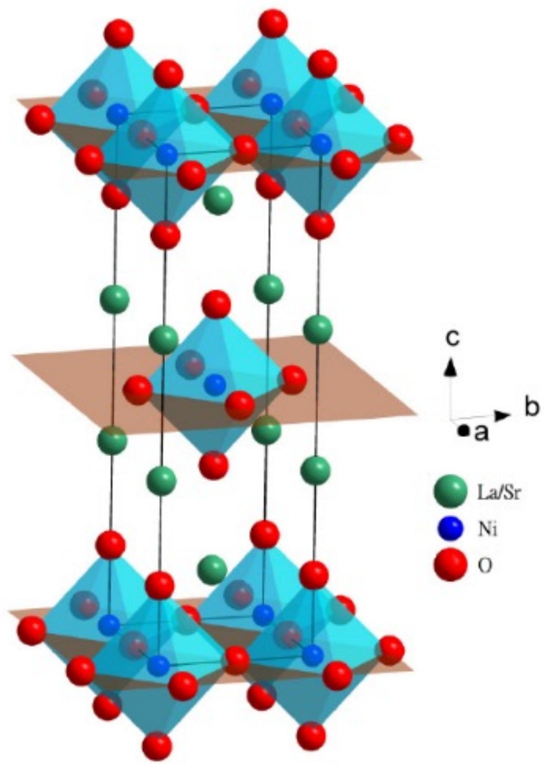

$La_{2-x}Sr_xNiO_4$

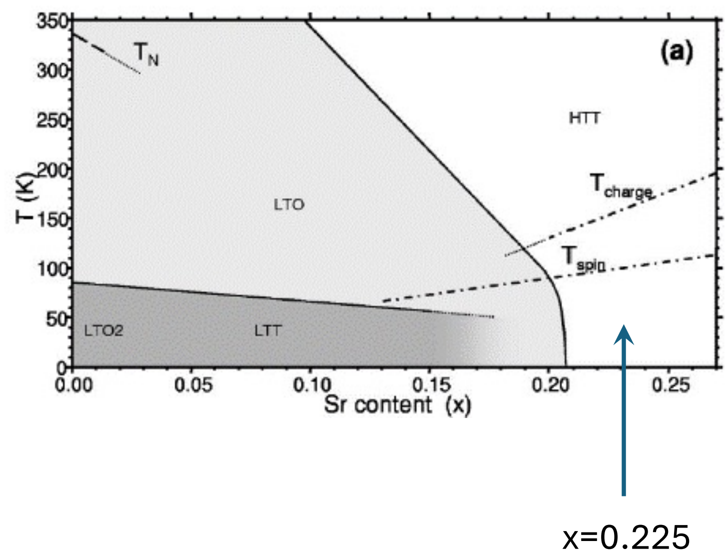

$La_{1.775}Sr_{0.225}NiO_4$ sample at CSX, NSLS-II

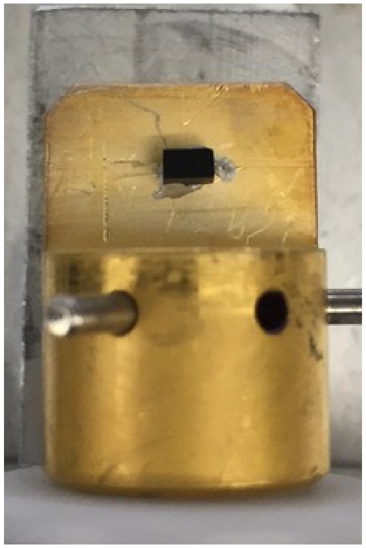

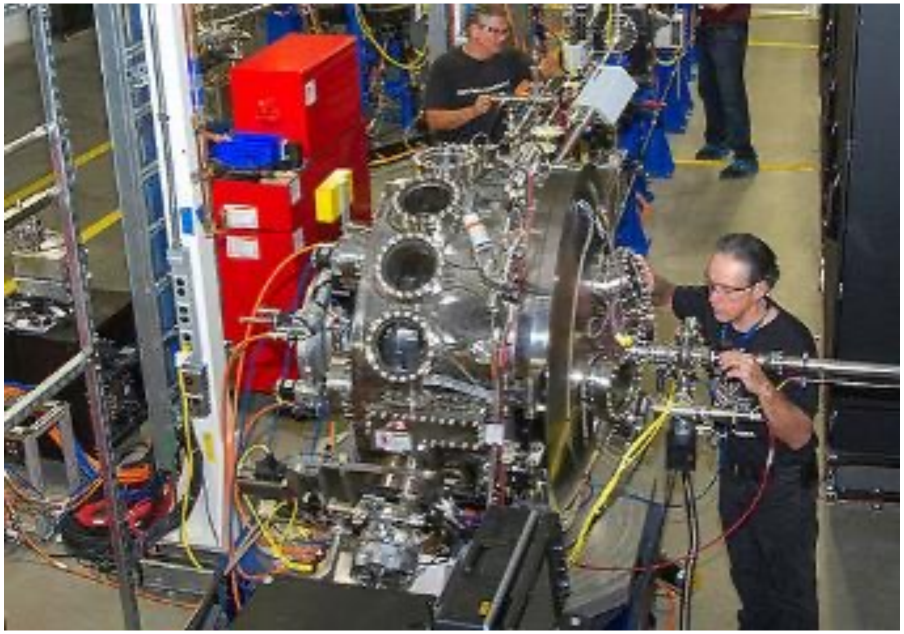

CSX Soft X-ray Coherence beamline at NSLS-II

Charge/spin order in $La_{1.775}Sr_{0.225}NiO_4$ Nickeate

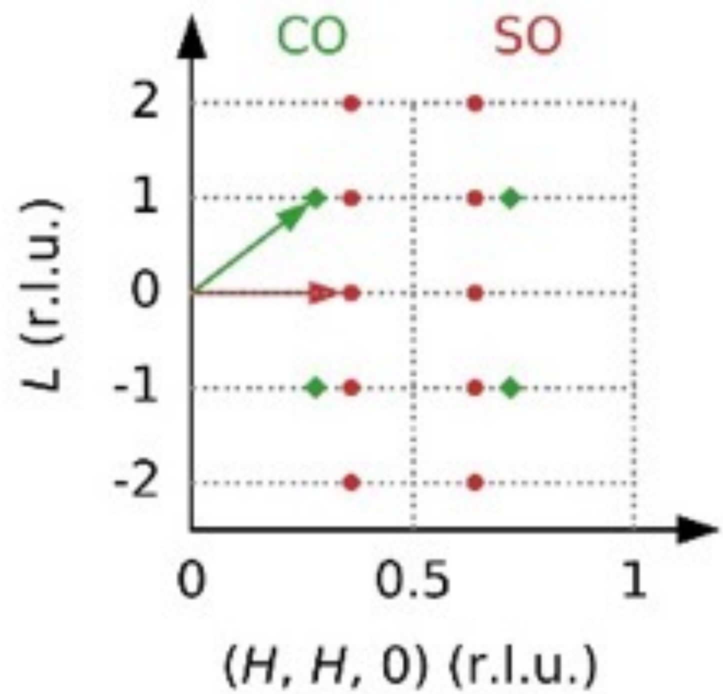

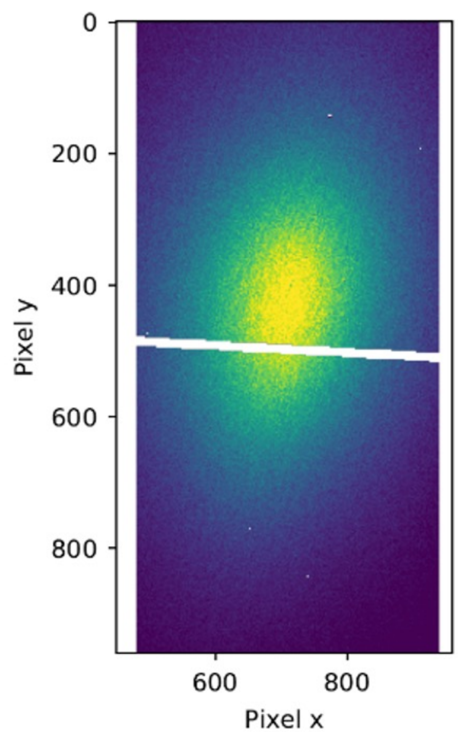

CO: (ϵ, ϵ, 1)

SO: (1/2 - ϵ/2, 1/2 - ϵ/2, 0)

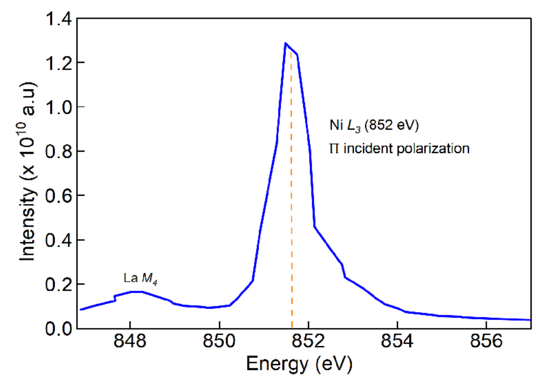

Y. Shen et al PRL 126 177601 (2021)
A. Mitra et al PRB (submitted)

Speckled Diffraction Charge/Spin order

CO (0.28, 0.28, 1)
SO (0.36, 0.36, 0)

Y. Shen et al. PRL 126 177601 (2021)

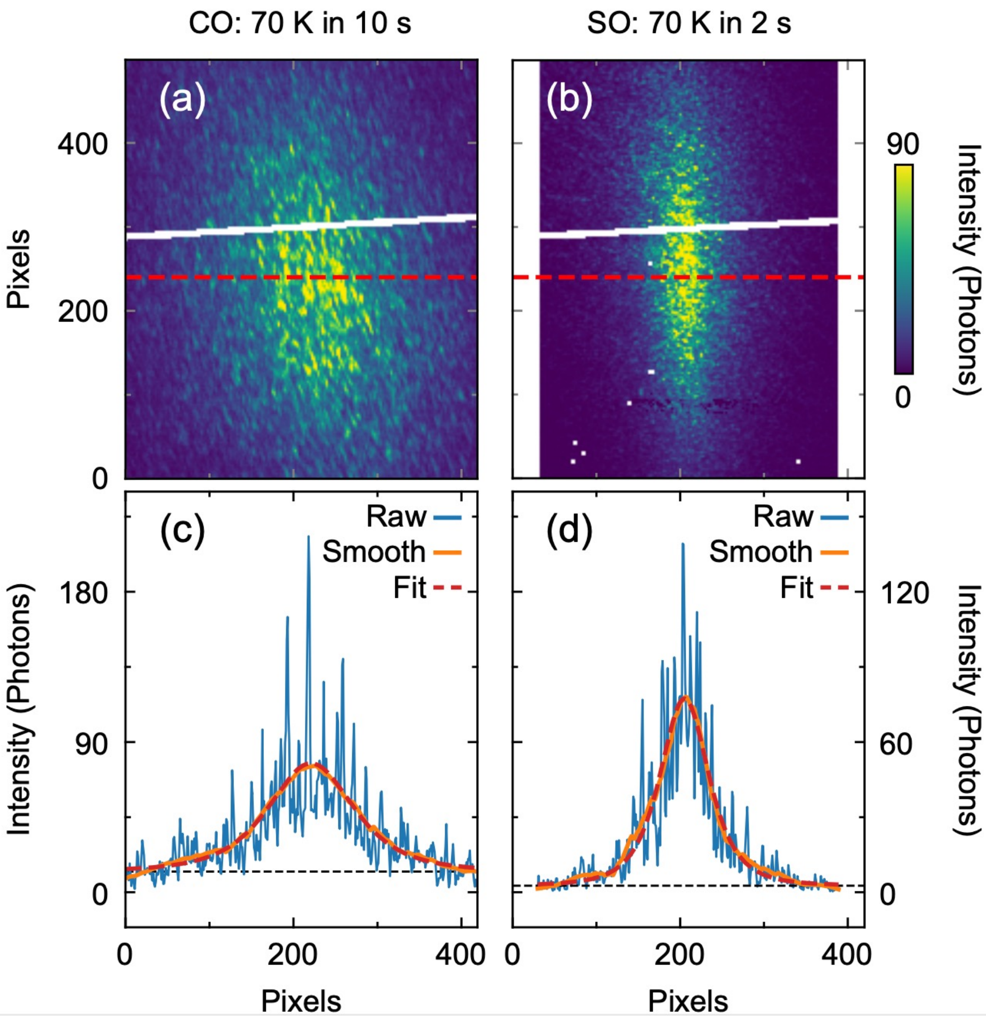

Striped Domains near Surface

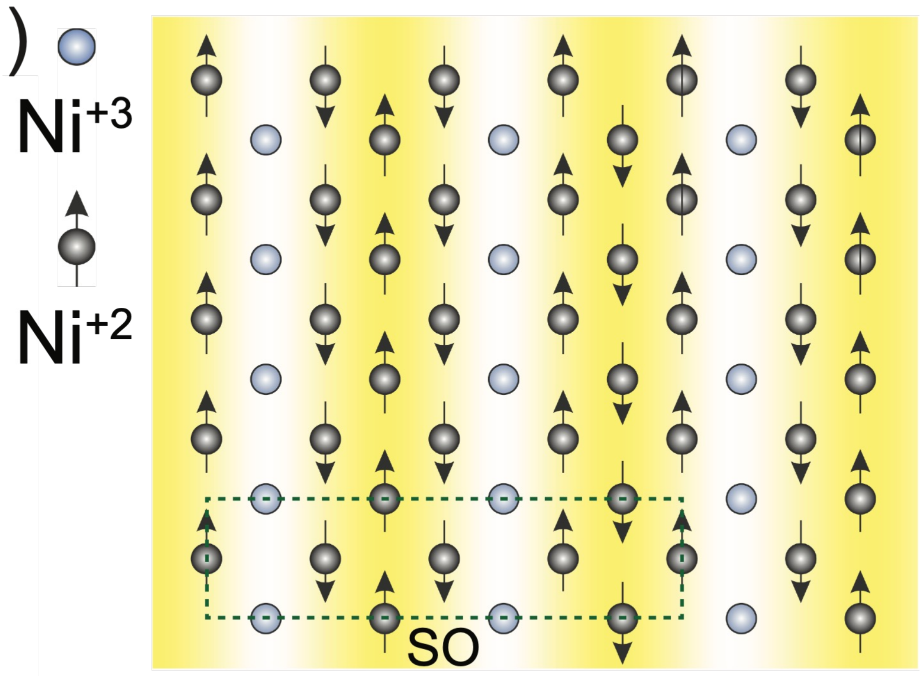

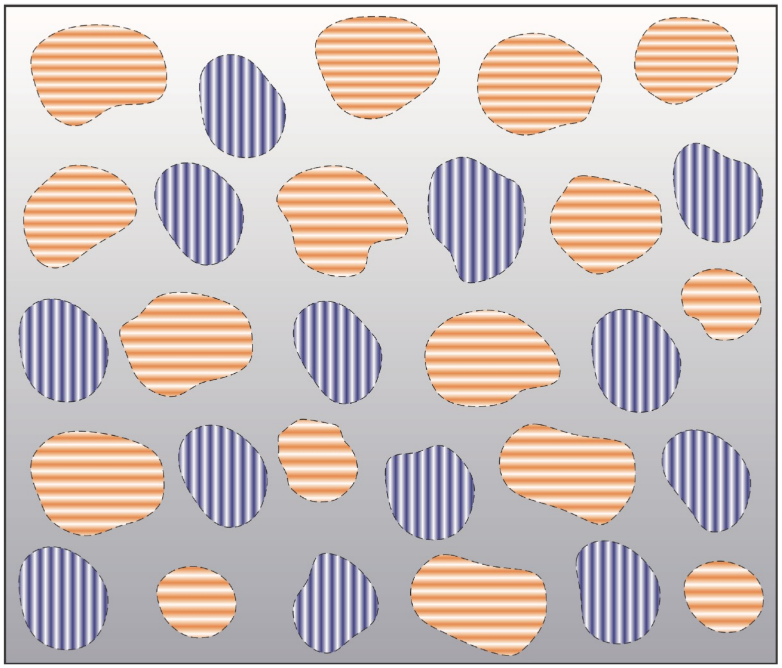

3D mapping of Spin-Order peak

Magnetic scattering at Ni L_3 edge, 852eV

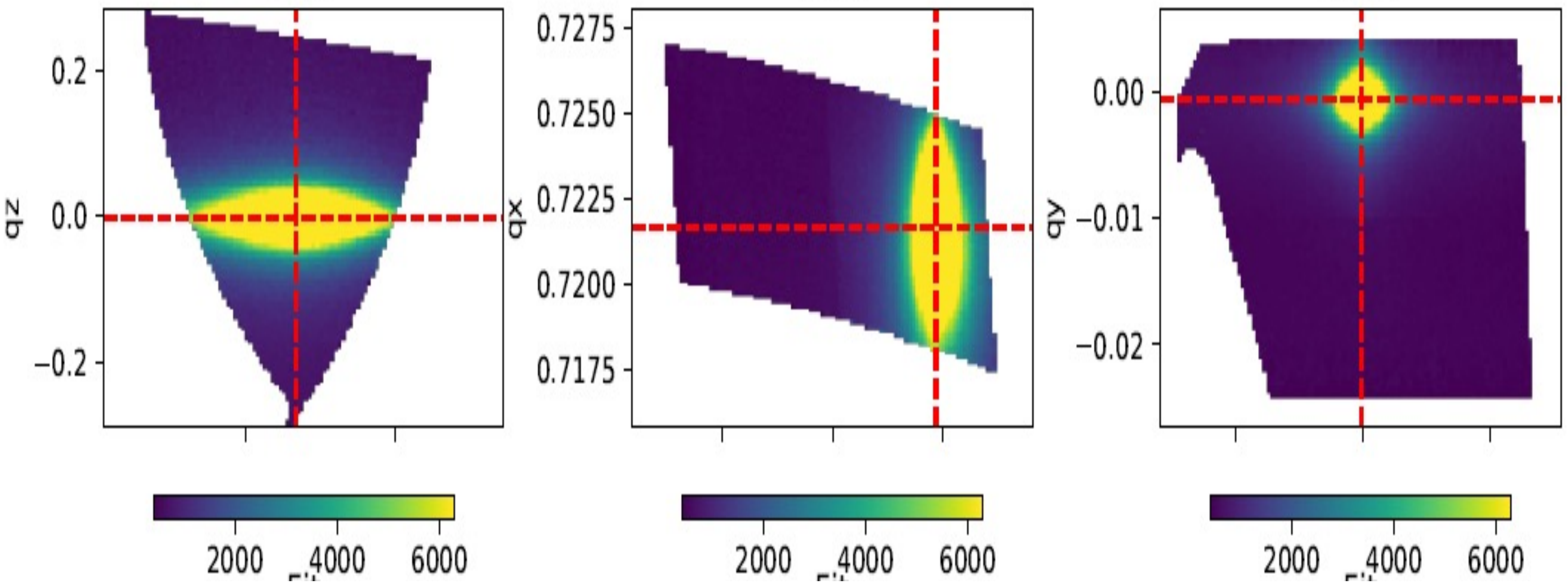

$La_{1.775}Sr_{0.225}NiO_4$ Correlation Length vs Temp

Y. Shen et al, Phys. Rev. Letts. 126 177601 (2021)

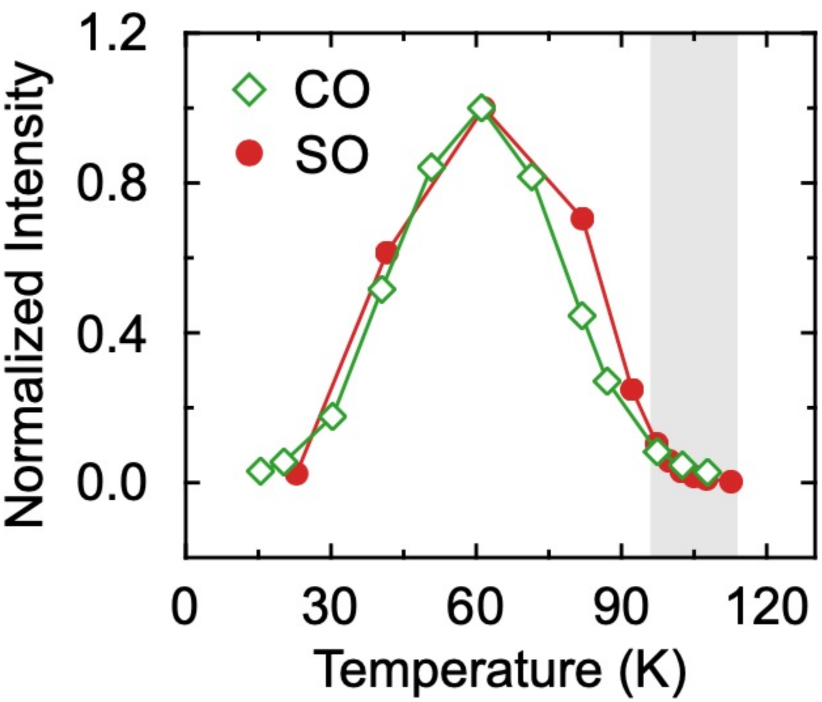

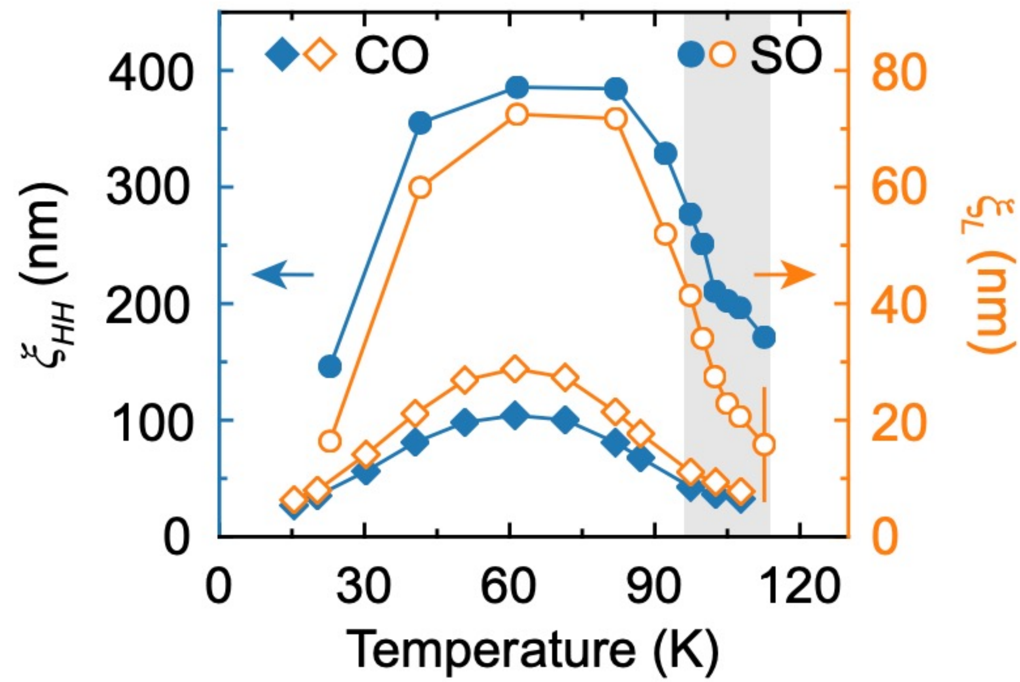

X-ray Photon Correlation Spectroscopy (XPCS)

Charge Condensation and Lattice Coupling Drives Stripe Formation in Nickelates Y. Shen et al Phys. Rev. Letts. 126 177601 (2021)

$$g_2(\boldsymbol{q},\tau) = \frac{\langle I(\boldsymbol{q},t)I(\boldsymbol{q},t+\tau)\rangle}{\langle I(\boldsymbol{q},t)\rangle^2} = 1 + \beta|F(\boldsymbol{q},\tau)|^2.$$

O. G. Shpyrko, J. Synch. Rad. 21, 1057 (2014)

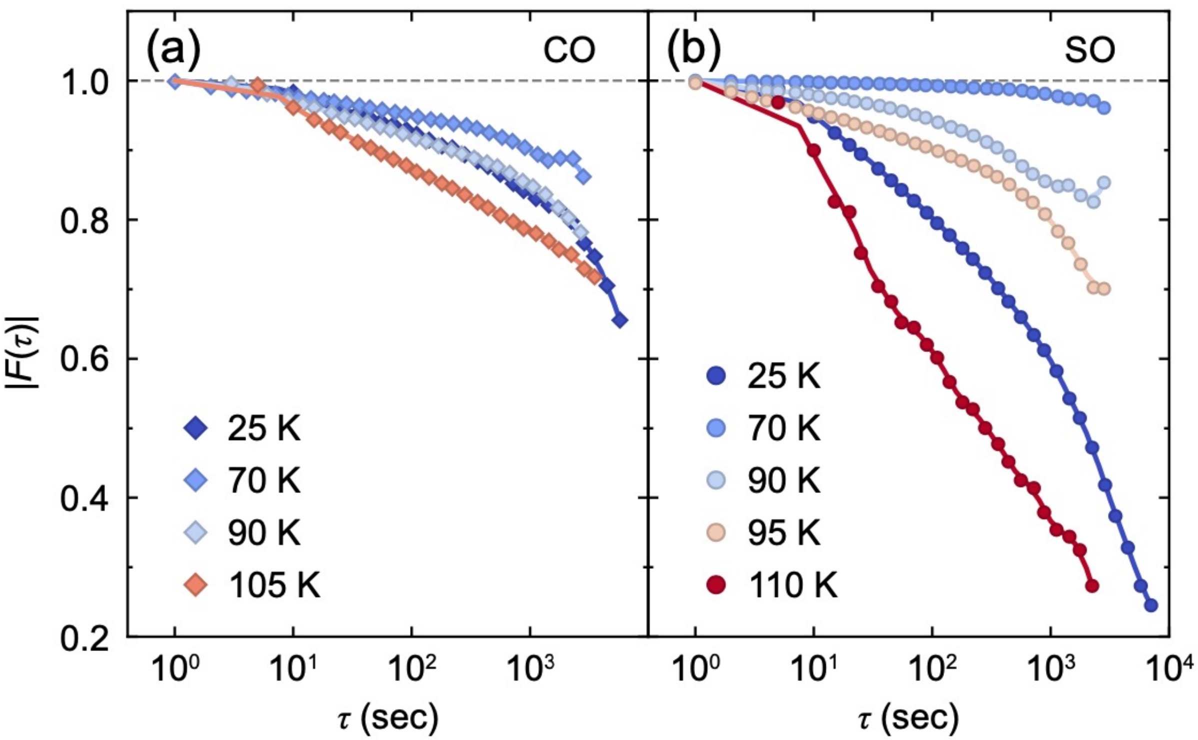

Bragg Ptycho with FIB-polished 8μm Pinhole

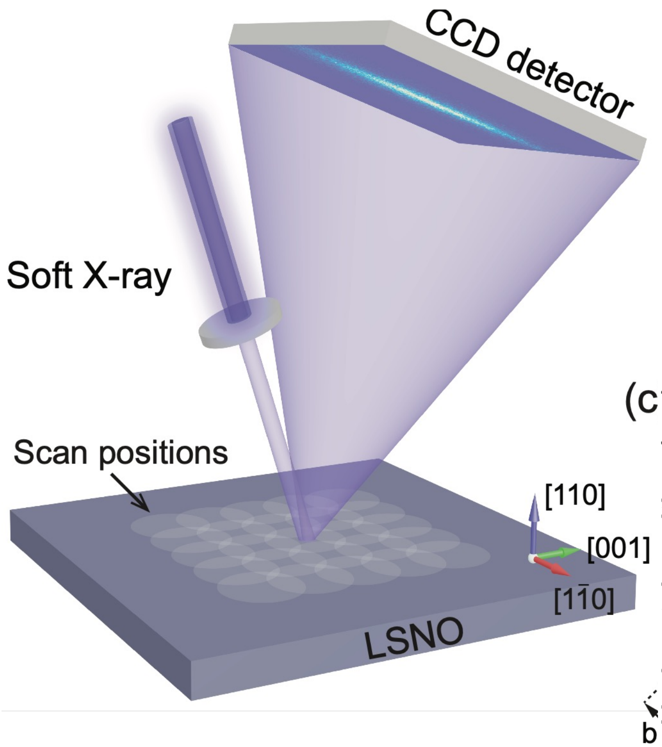

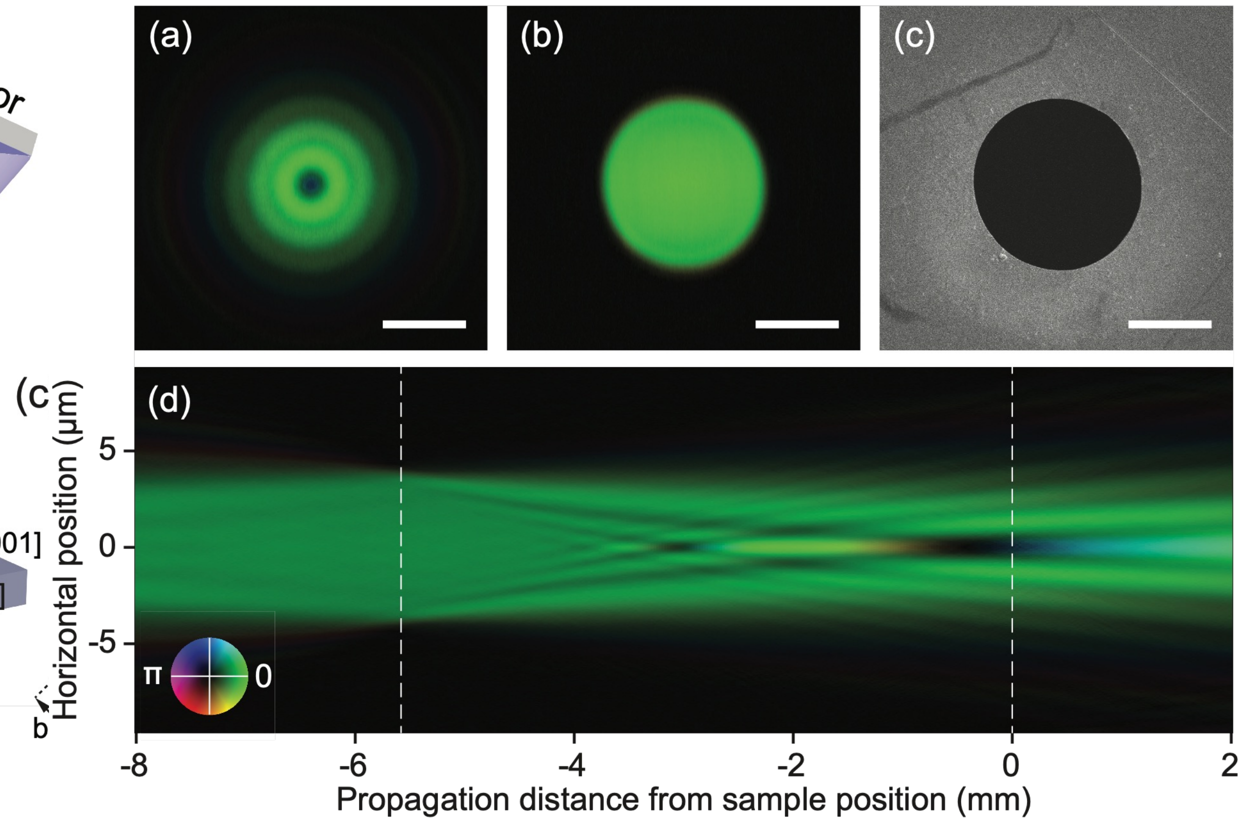

Full Size Ptychography Image $La_{1.775}Sr_{0.225}NiO_4$ (HSV coding)

Longlong Wu, Yao Shen et al, Phys. Rev. Lett **127** 275301 (2021)

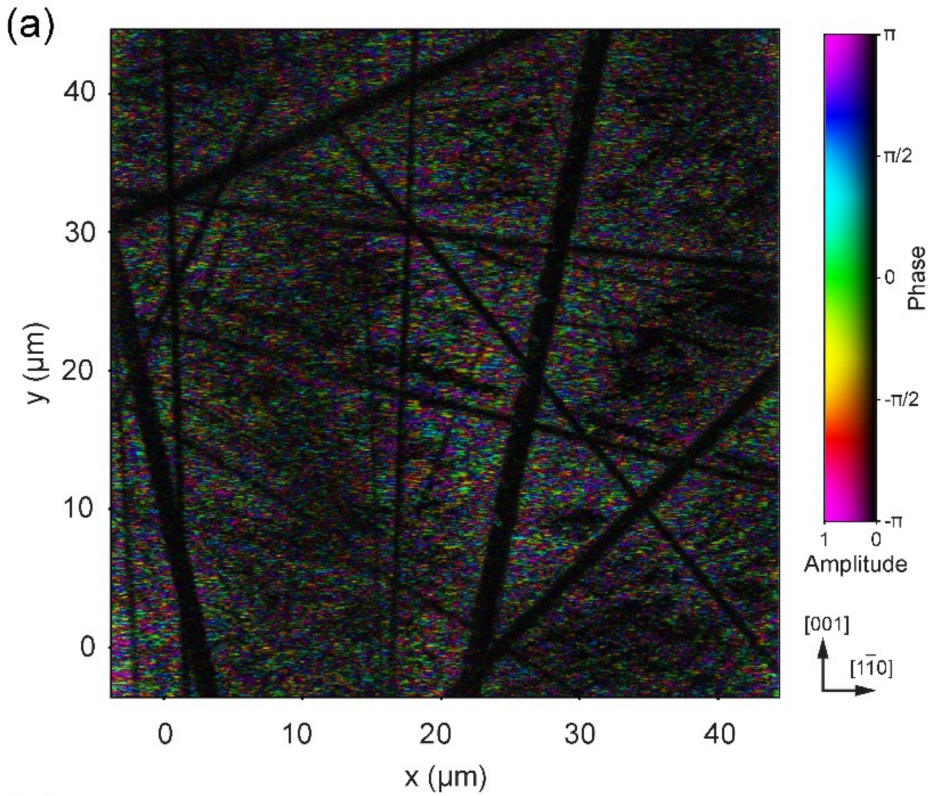

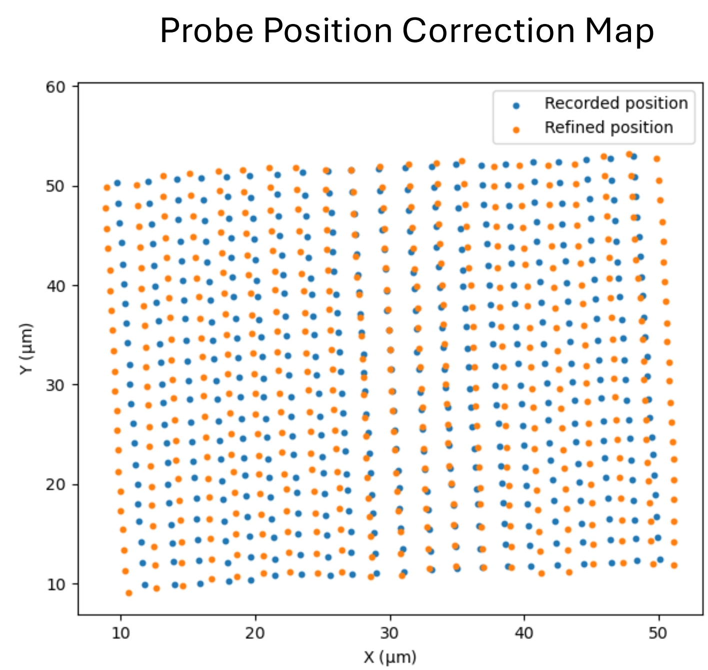

Time Series of domains at 70K. HSV coding

Longlong Wu, Yao Shen et al, Phys. Rev. Lett **127** 275301 (2021)

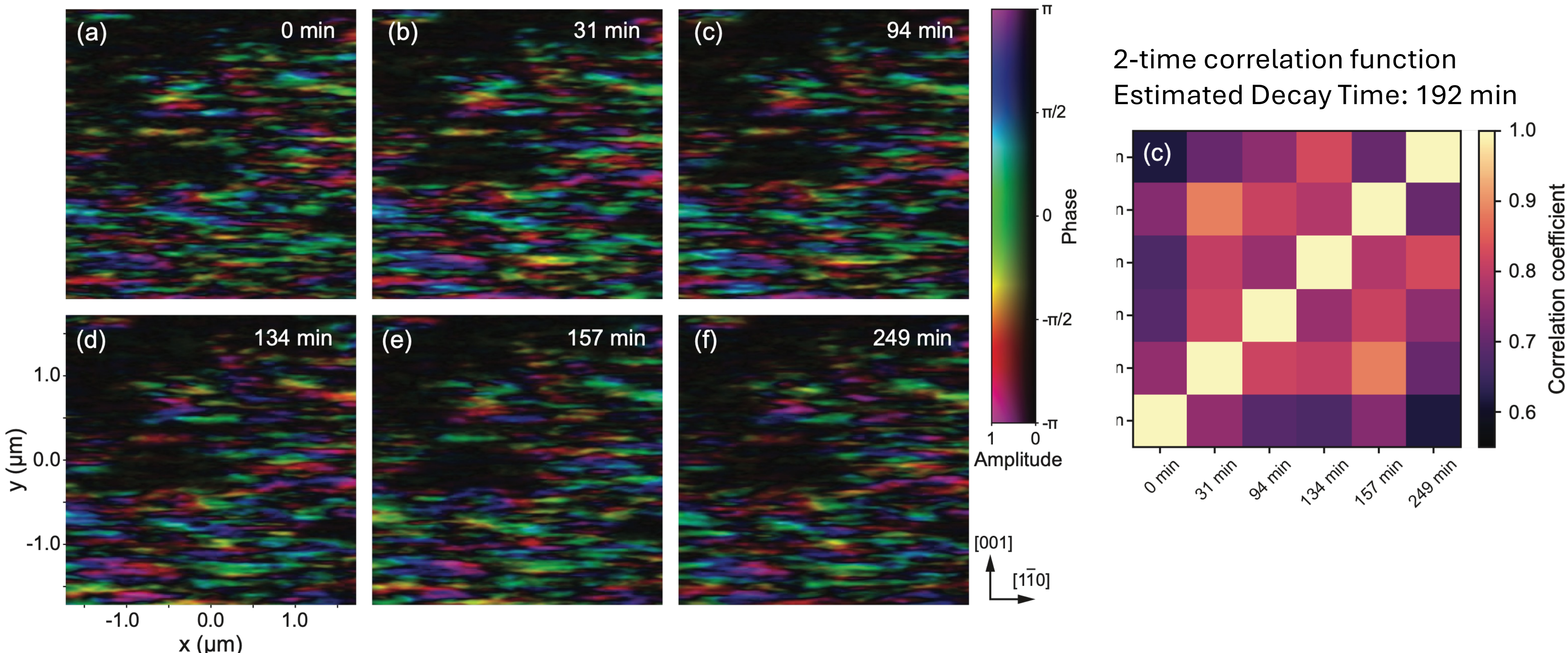

Hydrothermal Nano $BaTiO_3$ Dielectric BCDI

Tetragonal small-angle grain boundaries

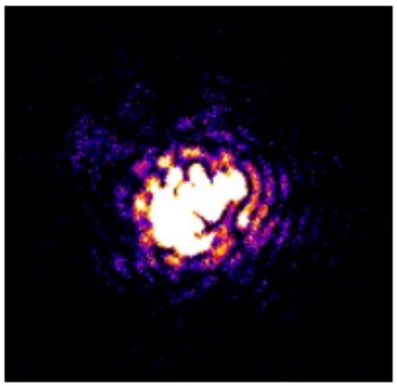

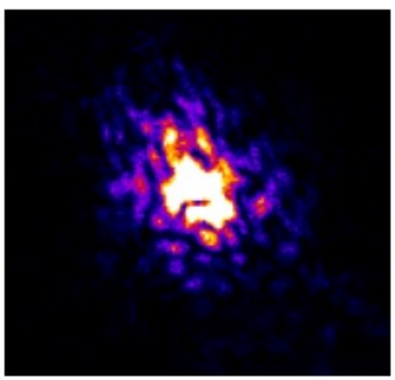

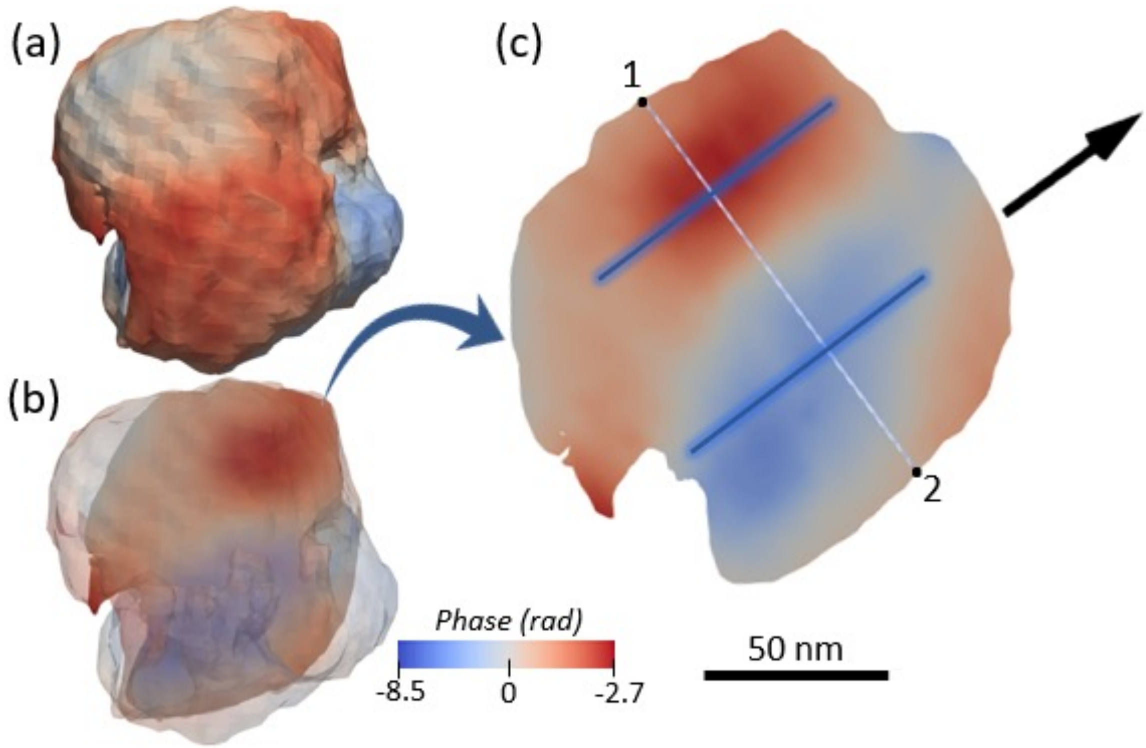

Nanoscale Merohedral Twinning

90º grain boundaries energetically favored

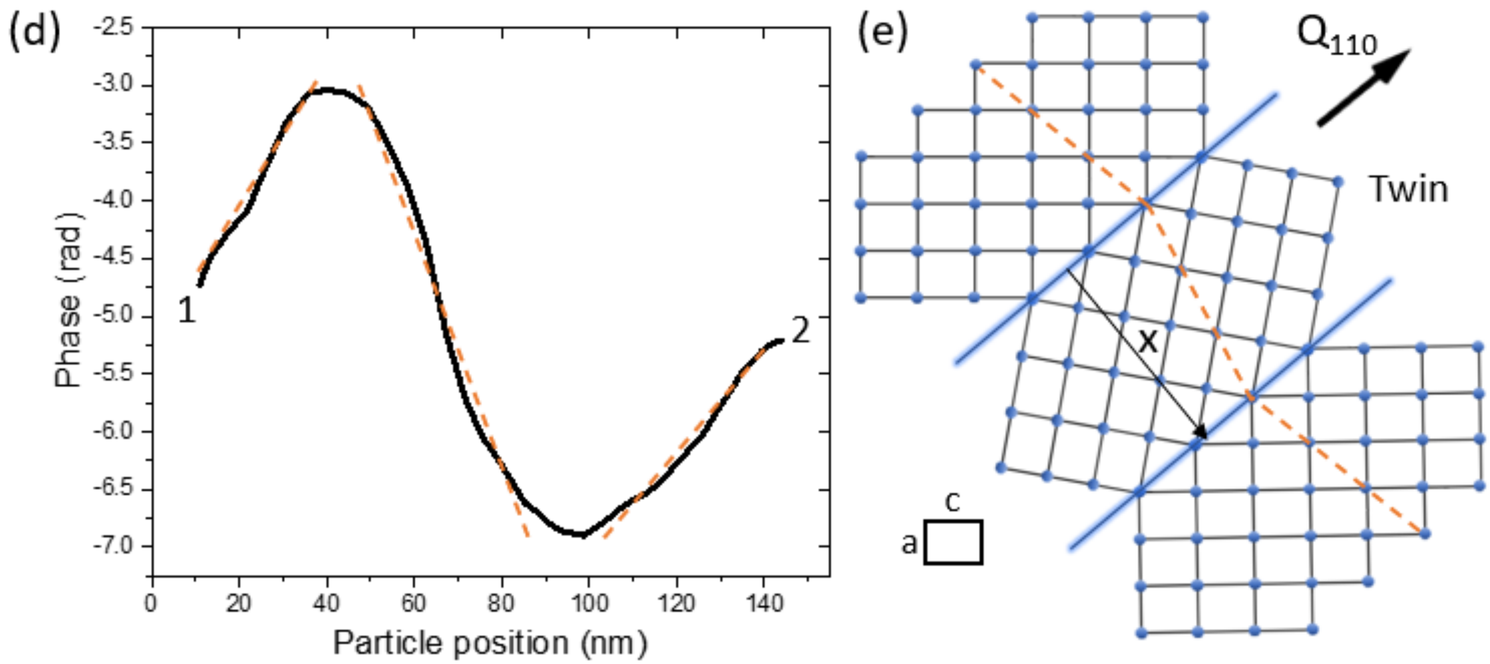

c/a = 1.0035 for observed change of slope

Ana F. Suzana et al, Adv. Func. Materials 2208012 (2023)

Field-movement of Phase Profiles along Line Cut

Jialun Liu et al, Phys. Rev. B 111 054101 (2025)

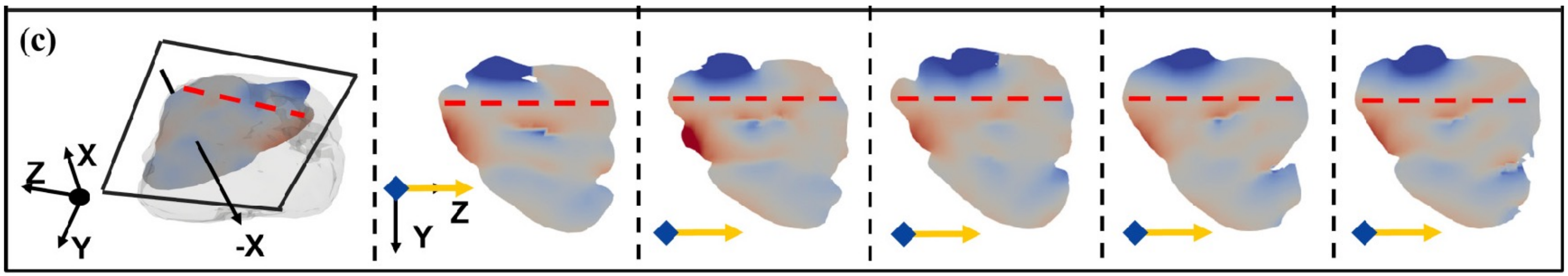

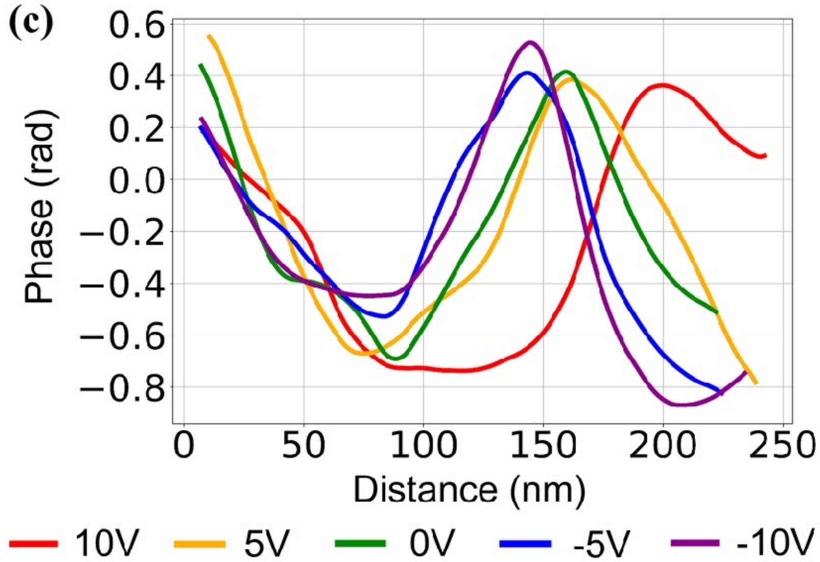

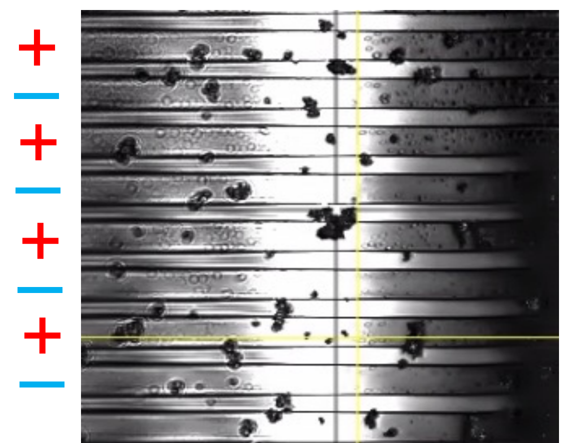

+/– 10V
3μm
spacing
3.3 MV/m

Multilayer Ceramic Capacitor uses $BaTiO_3$ nanoparticles

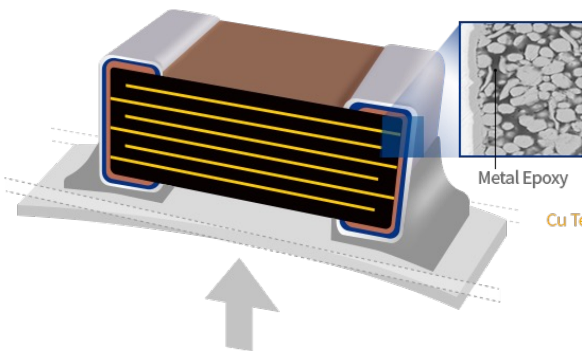

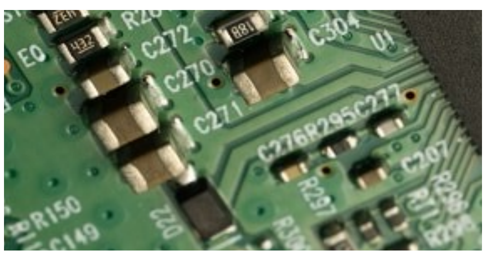

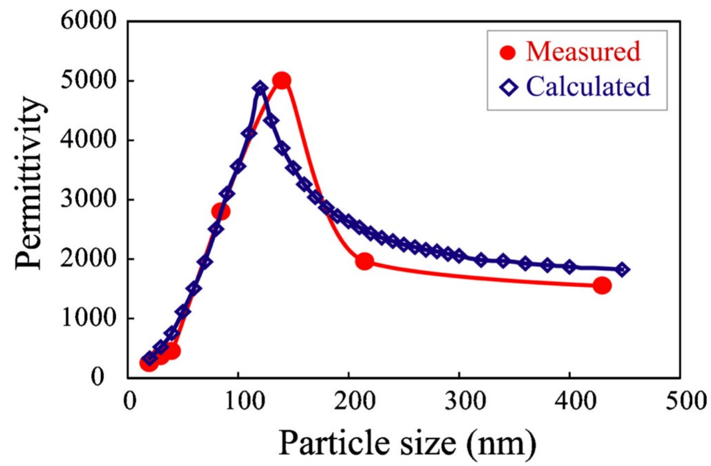

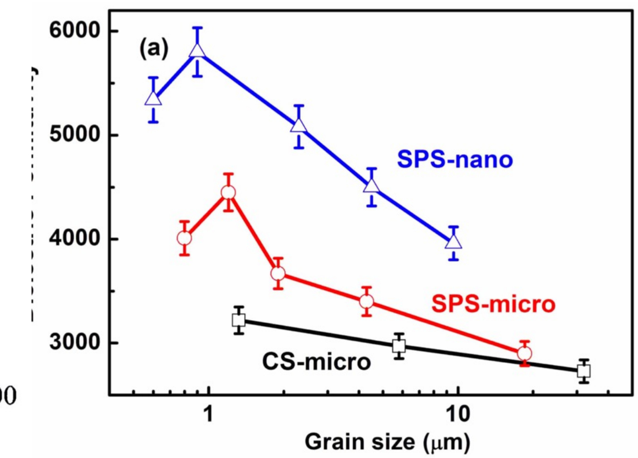

T. Hoshina, J. Ceramic Society of Japan **121** 156 (2013)
Y. Tan et al, Scientific Reports **5** 9953 (2015)
KEMET 22μF 16V part C2012X6S1C226M125AC
X6S dielectric is 90% nano $BaTiO_3$

High-Entropy halide Li_3InCl_6 Solid-State Electrolyte

Z. Song.., W. Luo, Nat. Comms **15** 1481 (2024)

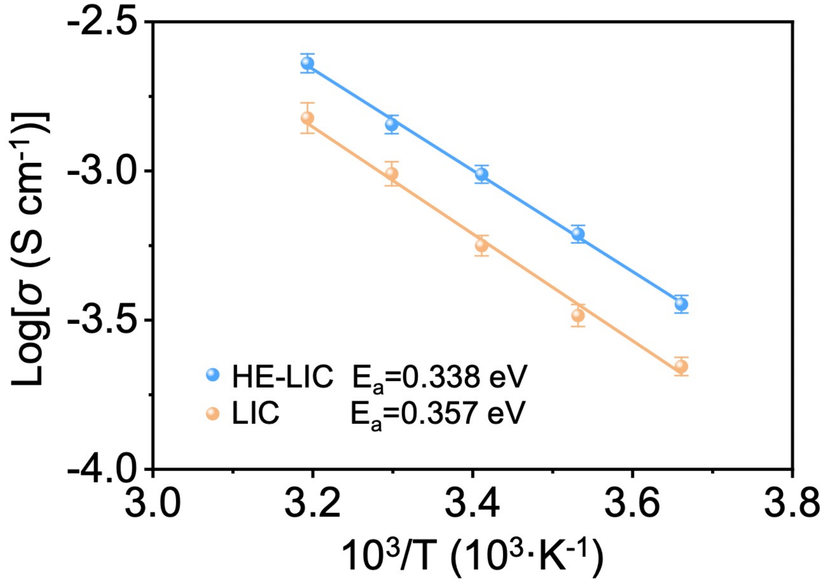

$Li_{2.75}Y_{0.16}Er_{0.16}Yb_{0.16}In_{0.25}Zr_{0.25}Cl_6$

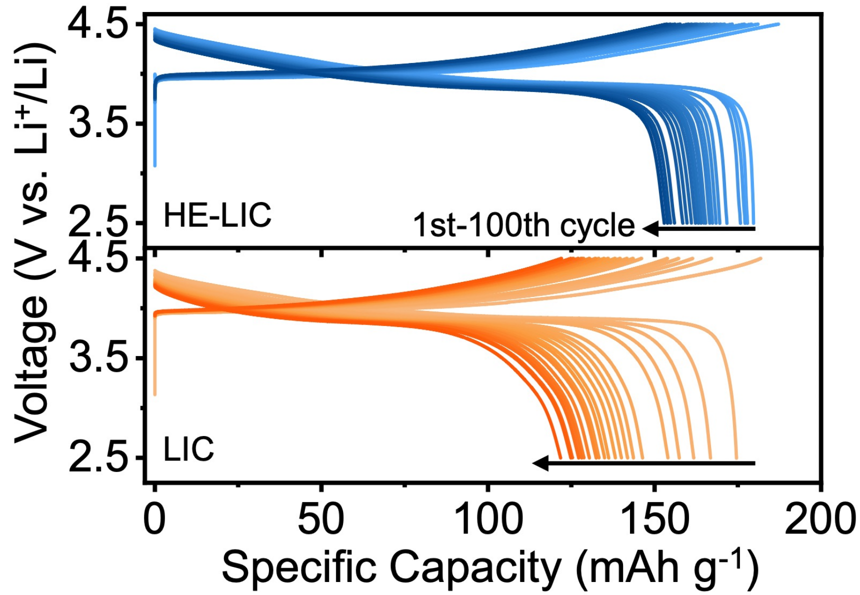

High-Entropy enhancement of Li-NASICON SSE

Y. Zeng, et al. Science **378** 1320 (2022)

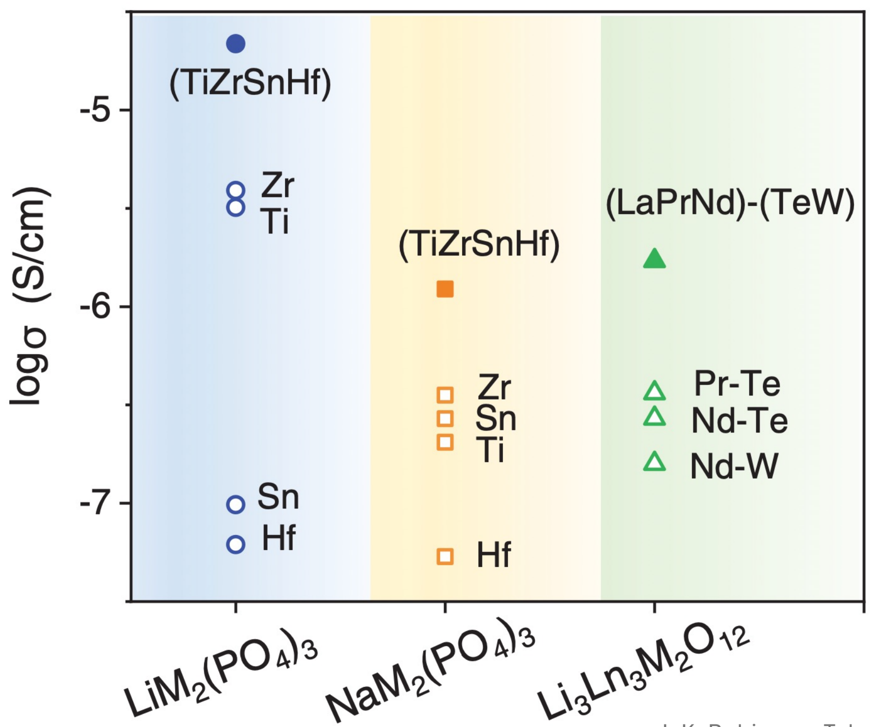

$Li(Ti,Zr,Sn,Hf)_2(PO_4)_3$

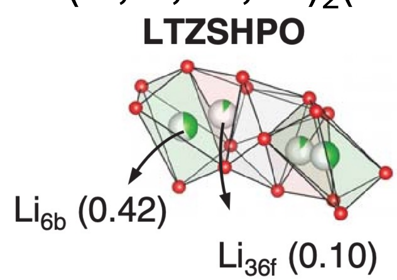

$Li_3(La,Pr,Nd)_3(Te,W)_2O_{12}$
garnet

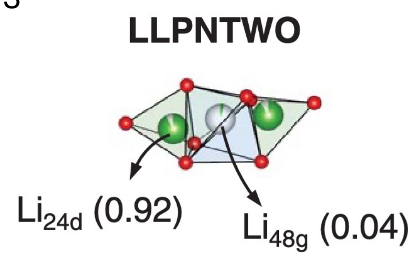

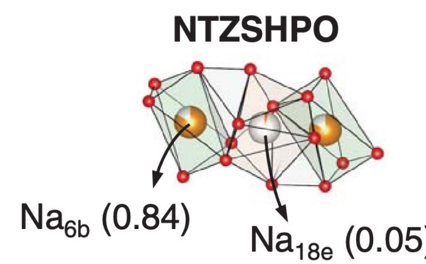

$Na(Ti,Zr,Sn,Hf)_2(PO_4)_3$

Systematic series with increasing substitution

Low Entropy	$LiTi_2(PO_4)_3$	$\sigma = 10^{-6}$ S/cm
Medium Entropy	$Li_{1.3}Al_{0.3}Ti_{1.7}(PO_4)_3$	$\sigma \sim 10^{-4}$ S/cm
High Entropy	$Li_3Ca_{0.5}Ti_{0.5}Zn_{0.5}Sn_{0.5}(PO_4)_3$	$\sigma \sim 10^{-3}$ S/cm

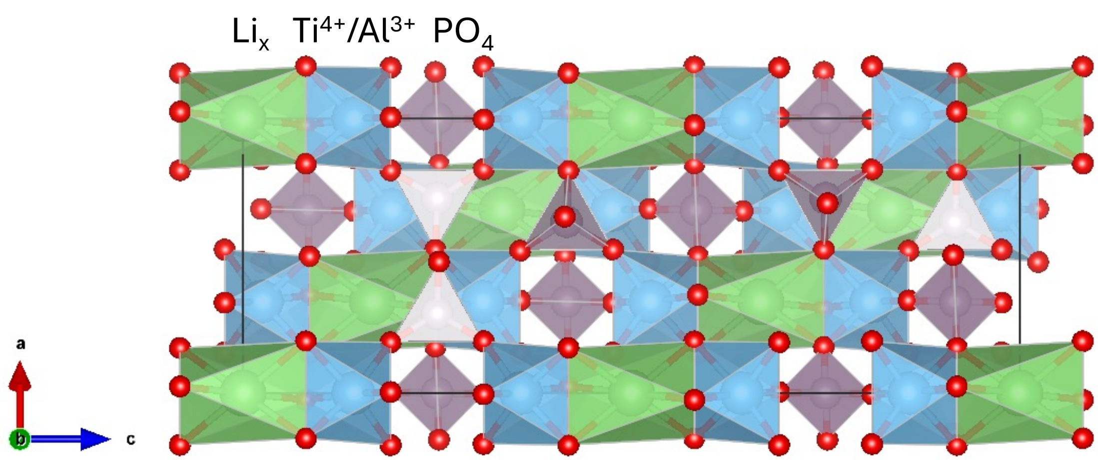

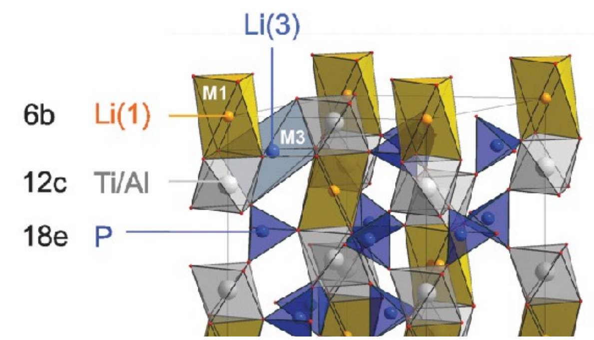

V. Epp et al, Phys. Chem. Chem. Phys. **17** 32115 (2015)
"Li stuffing" model

CM3-68F High-Entropy $Li_3Ti_2(PO_4)_3$ SSE

$Li_3Ca_{0.5}Ti_{0.5}Zn_{0.5}Sn_{0.5}(PO_4)_3$

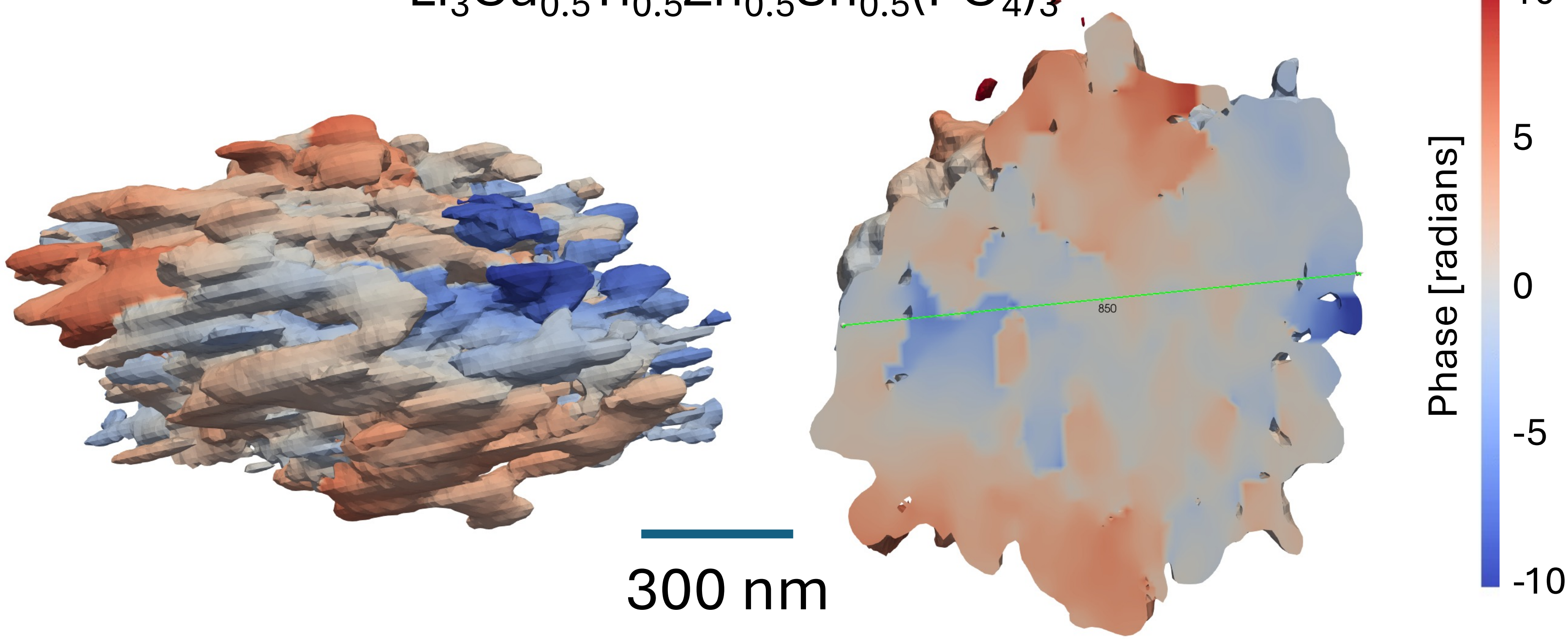

CM2 Medium-Entropy $Li_3Ti_2(PO_4)_3$ SSE

$Li_{1.3}Al_{0.3}Ti_{1.7}(PO_4)_3$

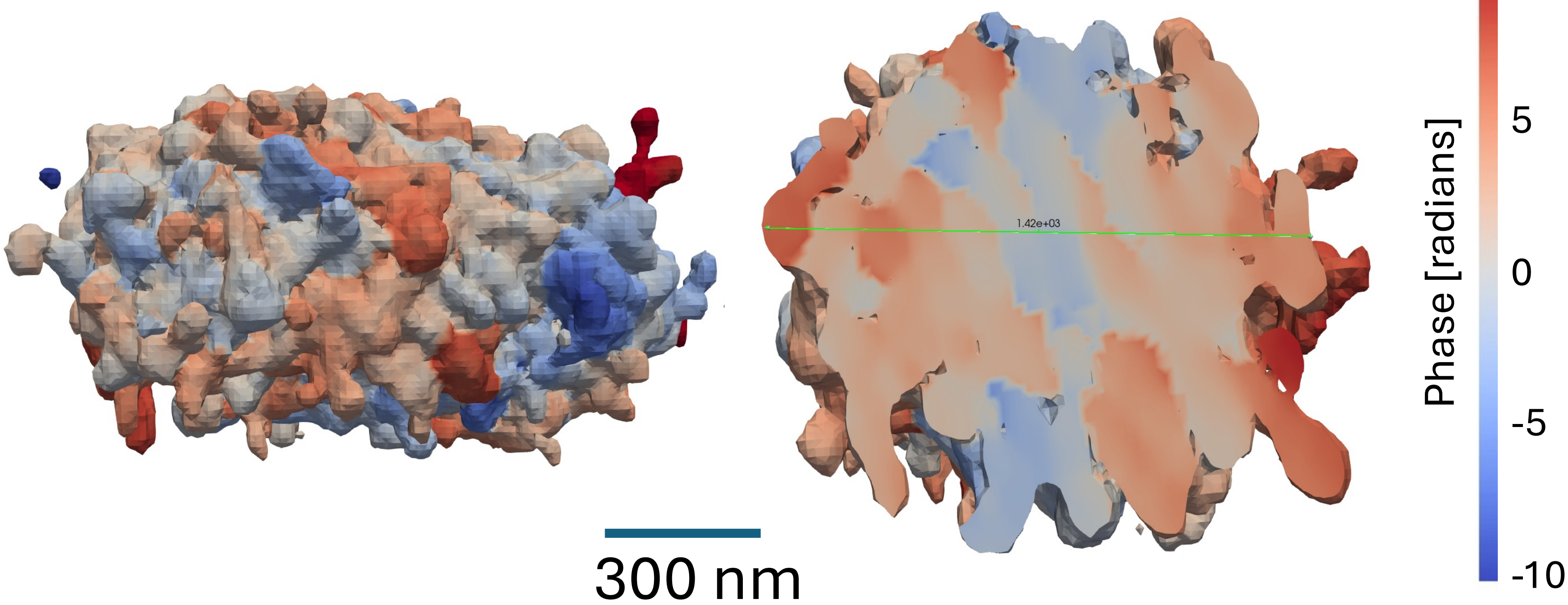

CM1-221 Low-Entropy $Li_3Ti_2(PO_4)_3$ SSE

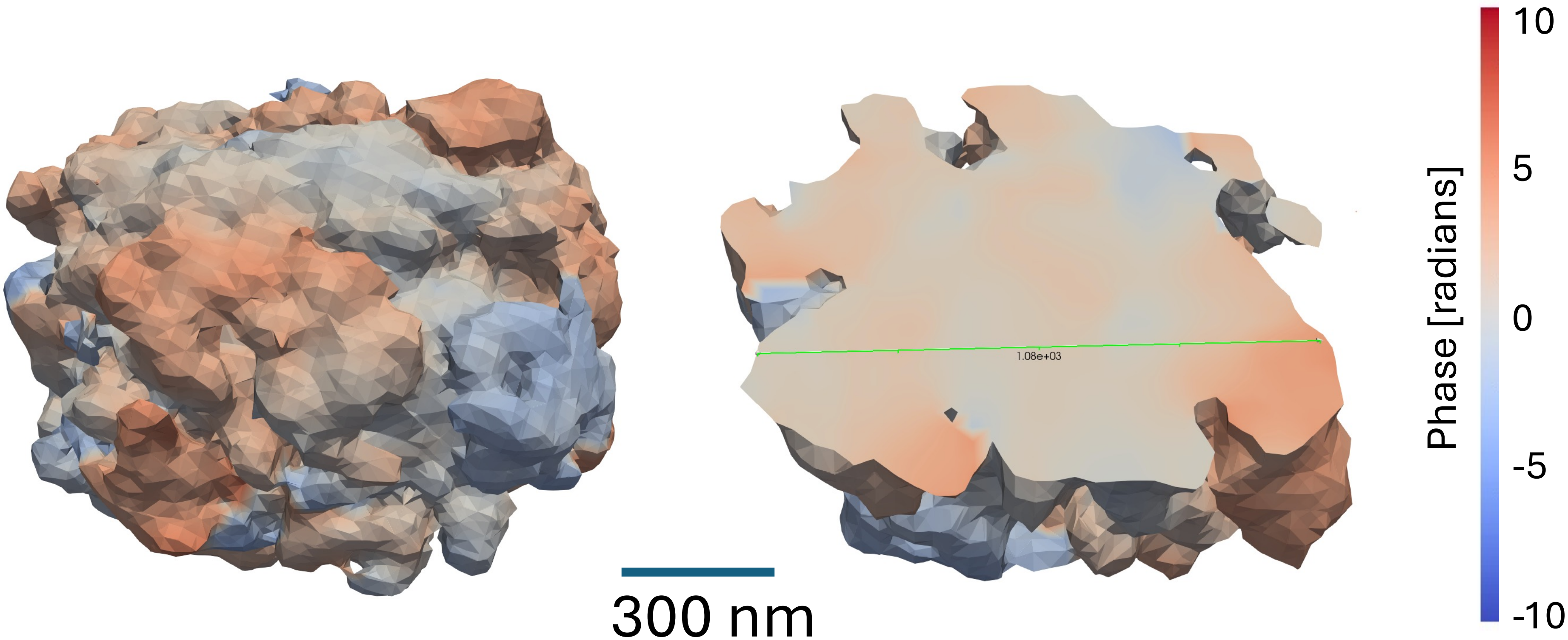

Domain-boundary conduction pathway?

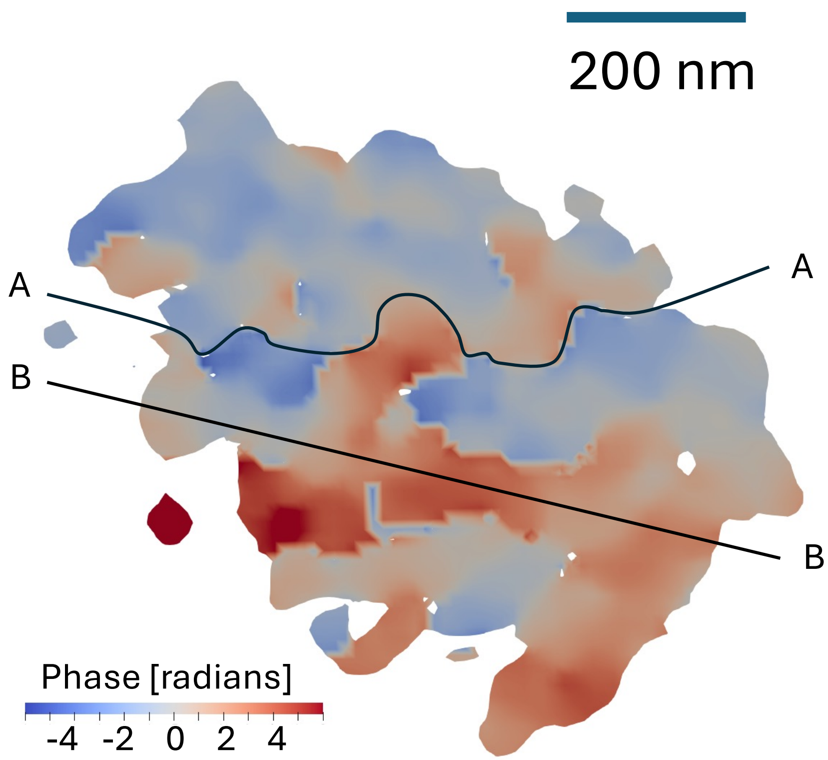

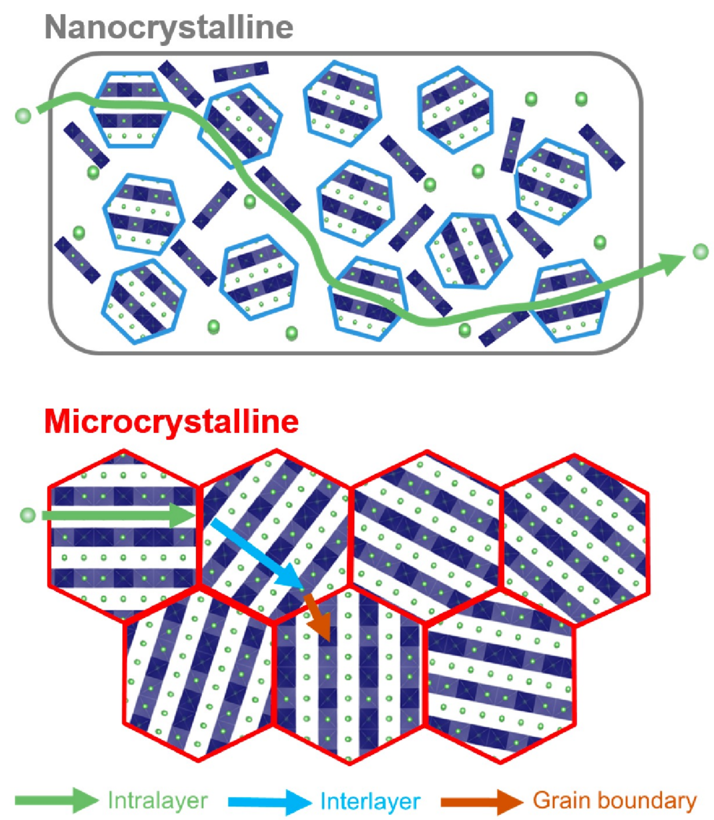

$Li_{3(1+x)}AlP_2$ J. Hu, et al J. Mater. Chem. A (2025)

Coherent X-ray Diffraction Imaging

- Phase Domains in materials
- Coherent Diffraction Imaging (CDI)
- Bragg ptychography
- Spin-ordered domains in $La_{2-x}Sr_xNiO_4$
- $BaTiO_3$ in Multilayer Capacitors
- Domains in solid state electrolyte crystals
- Opportunities for CDI at NanoTerasu

“Diffract and Destroy” setup

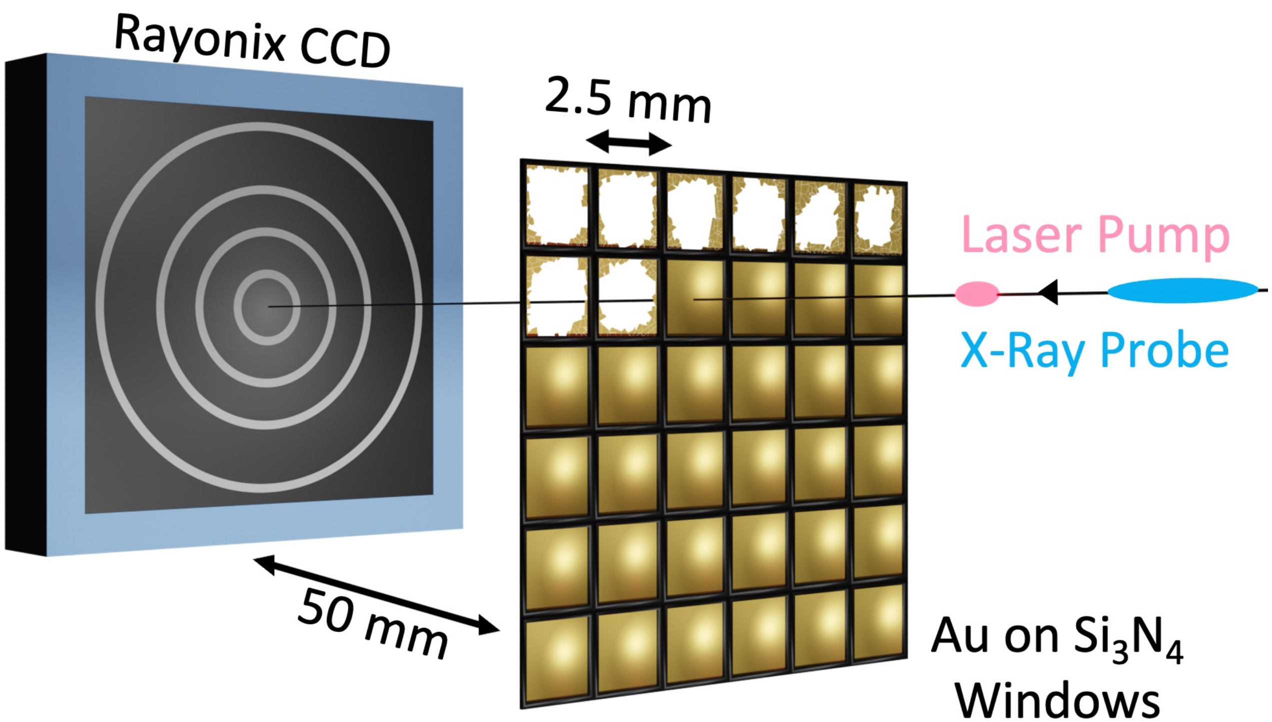

Scan Stage for MAXIC chamber with Silson arrays

Changyong Song et al, J. Appl. Cryst. **47** 188 (2014)
Daewoong Nam, scanning software

(b)

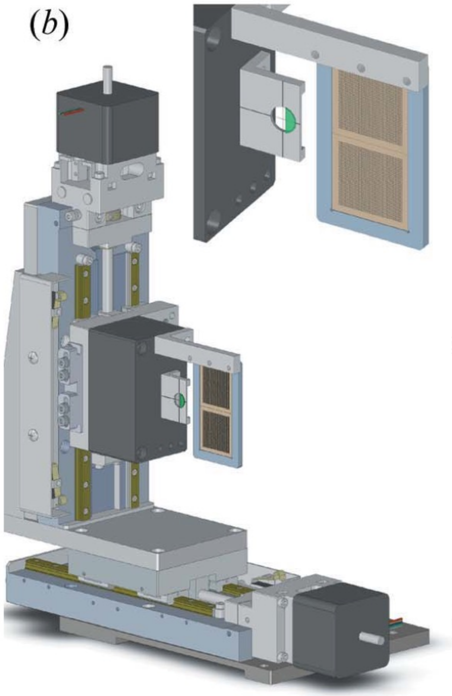

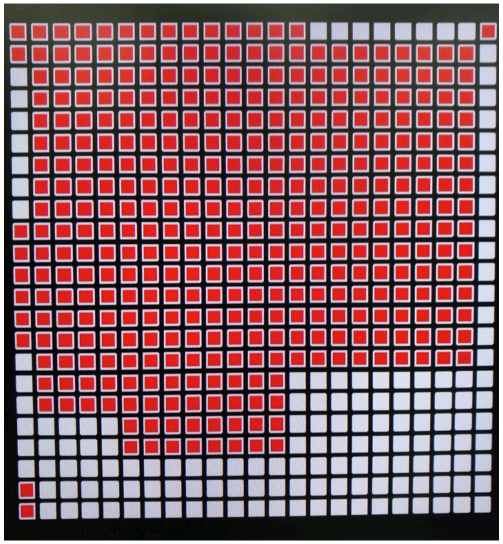

23x23 windows

Experimental set-up at PAL-XFEL September 2017

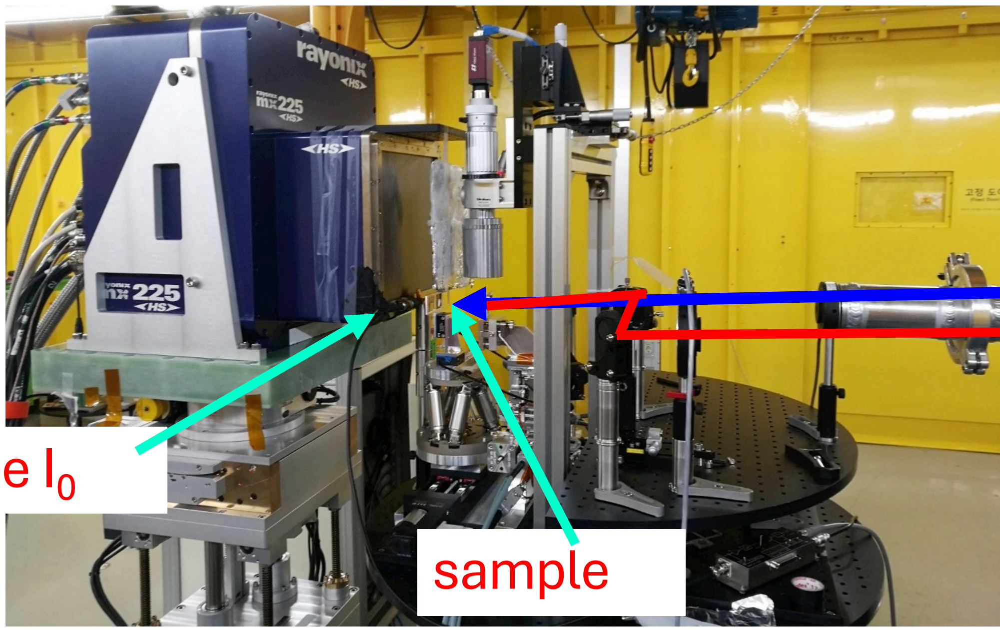

Raw data #397 300nm film

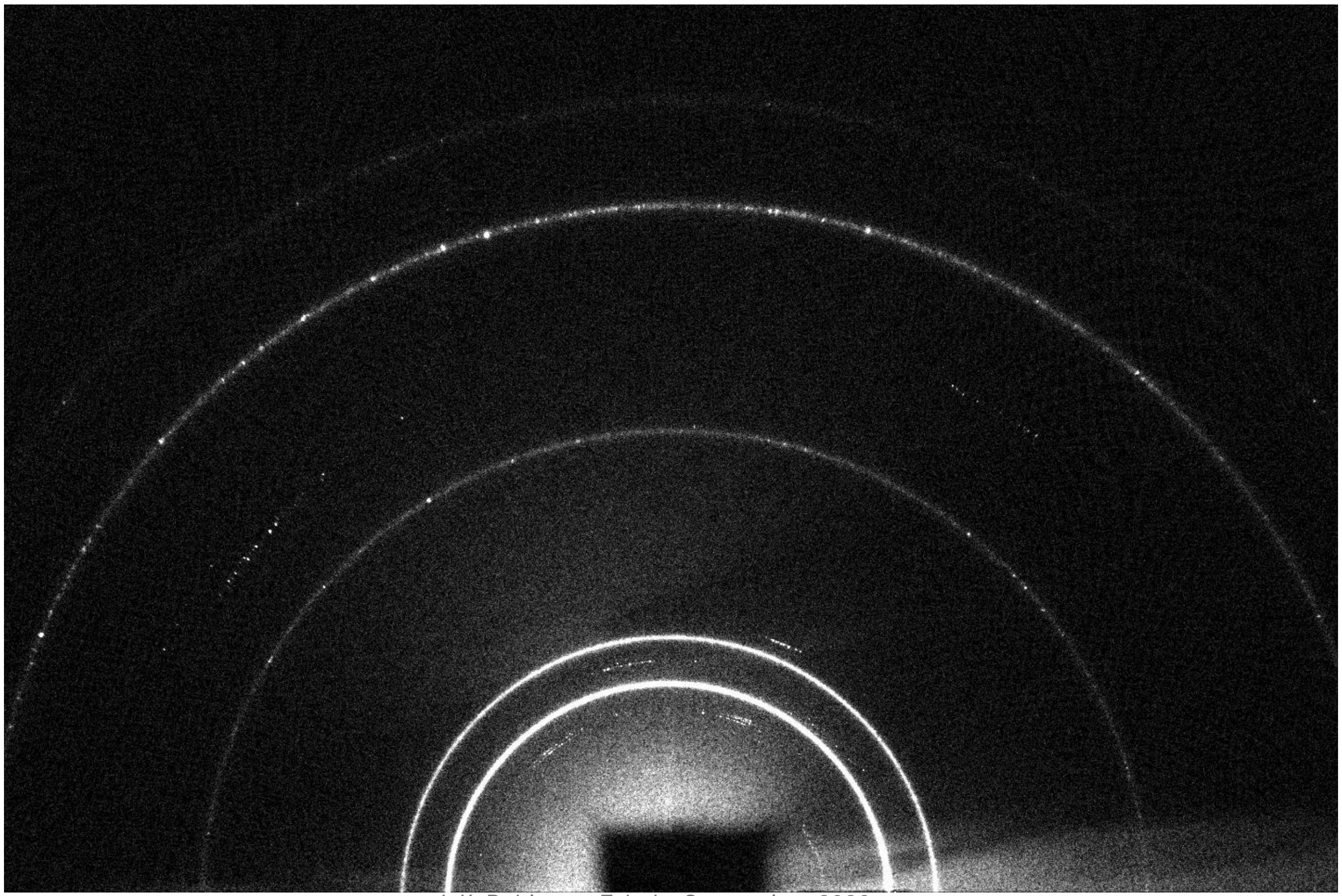

Raw data #396 300nm film, 254 mJ/cm^2

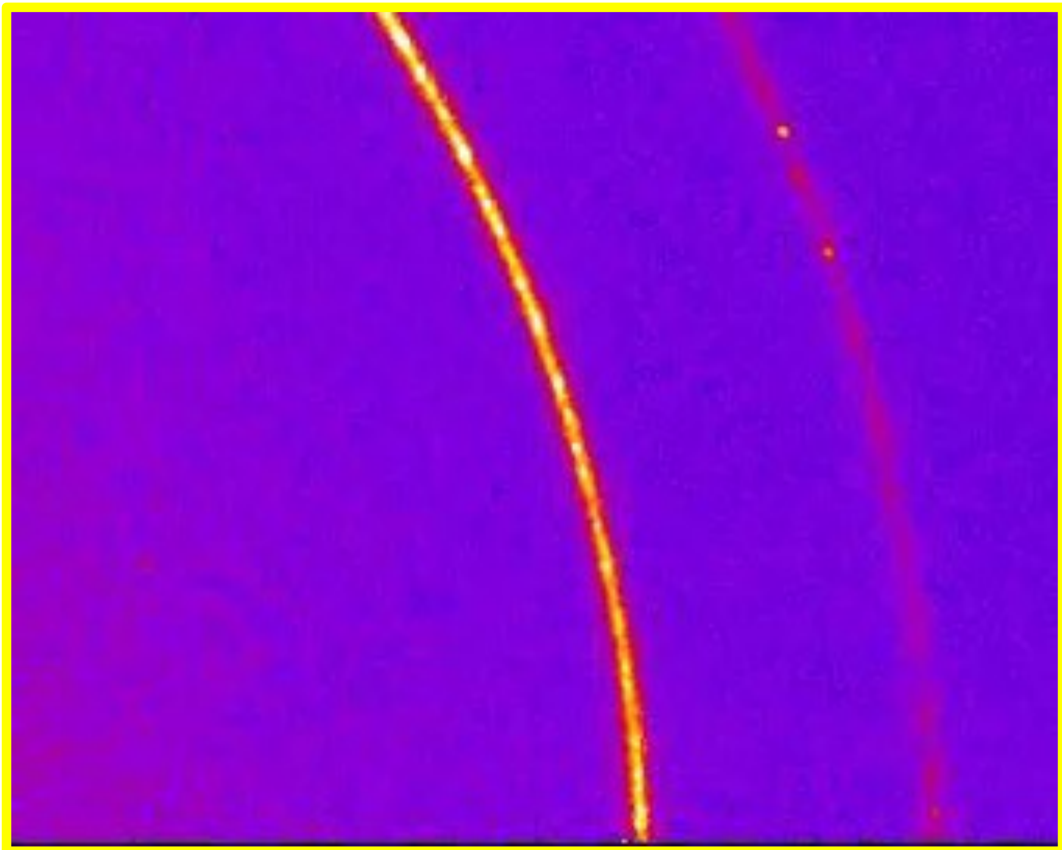

111 Powder Ring at 254 mJ/cm^2

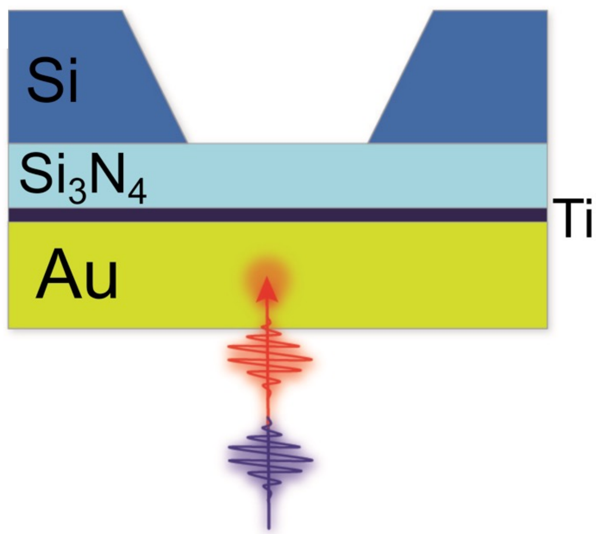

300 nm Au film

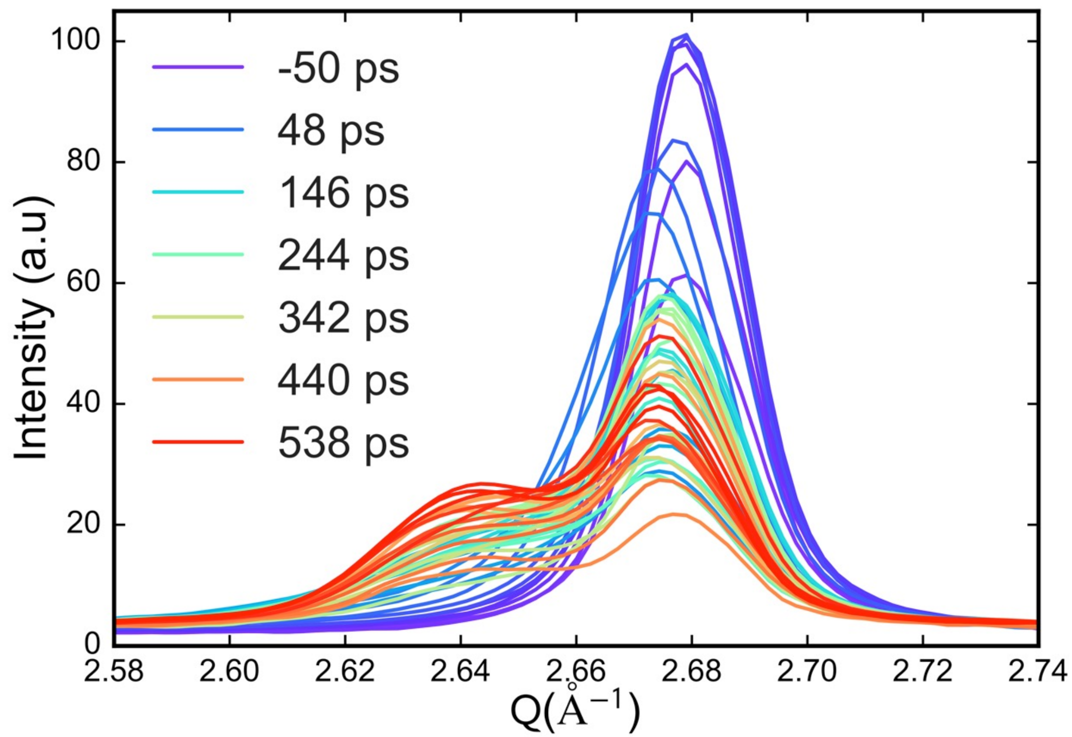

clearly inhomogeneous

Drude Resistivity of Al Thin Films

A. F. Mayadas and M. Shatzkes, PRB **1** 1382 (1970)

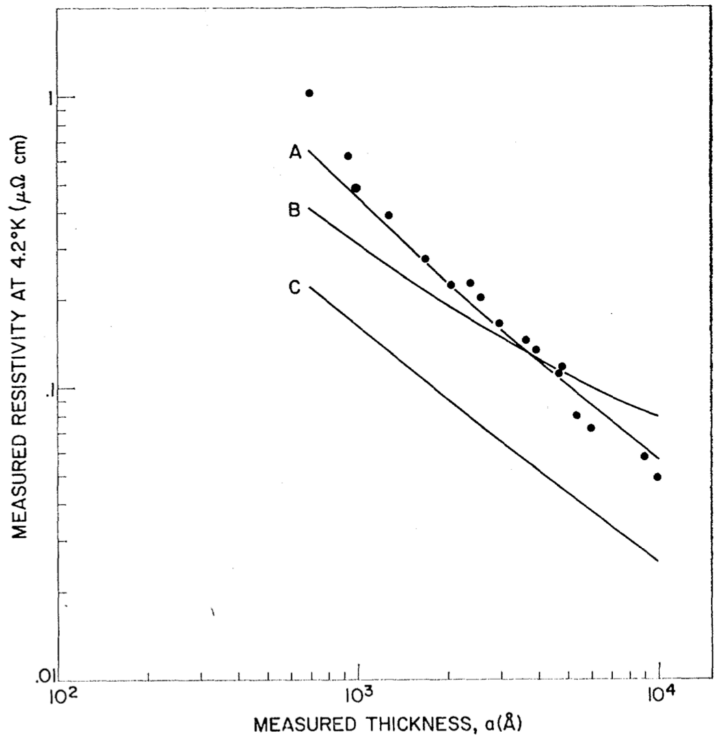

- "Universal curve" of Mean Free Path vs electron energy
- Thermal contribution to MFP removed at low temperature
- Grain size proportional to thickness (model)

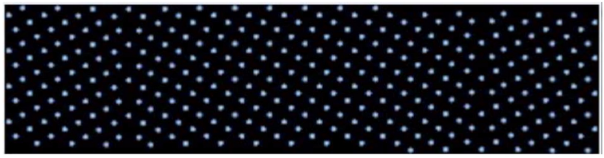

“Two-temperature” model

I.K. Robinson et al, Journal of Optics **18** 054007 (2016)
J.K. Chen et al, Int J. Heat Transfer **49** 307 (2006)

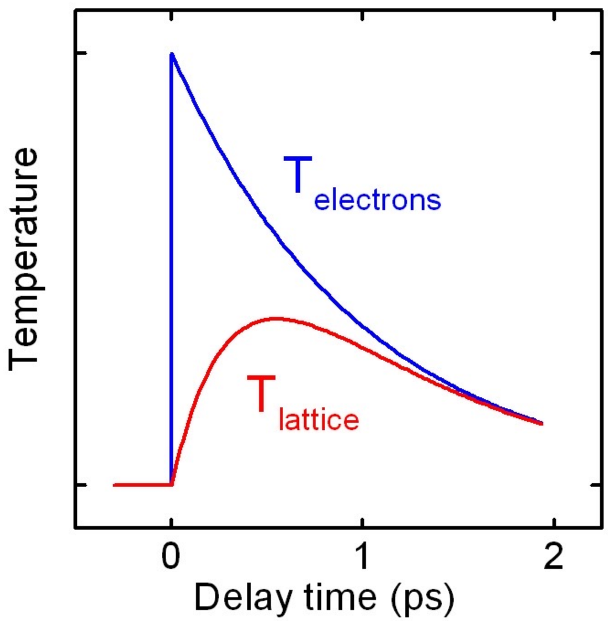

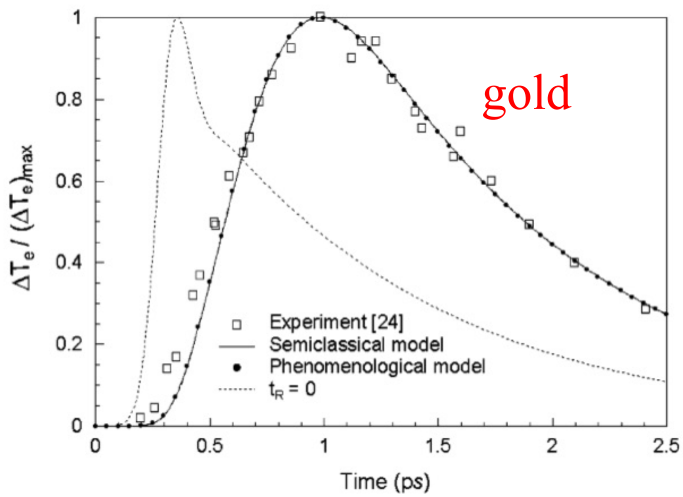

Fig. 2. Comparison of the change in electron temperature at the front surface of an 80-nm gold film irradiated by a 2.8 mJ/cm^2, 800 nm, 150-fs laser pulse.

2TM-MD (EAM) simulation of 10 nm Au slab

Giret et al, APL **103** 253107 (2013)

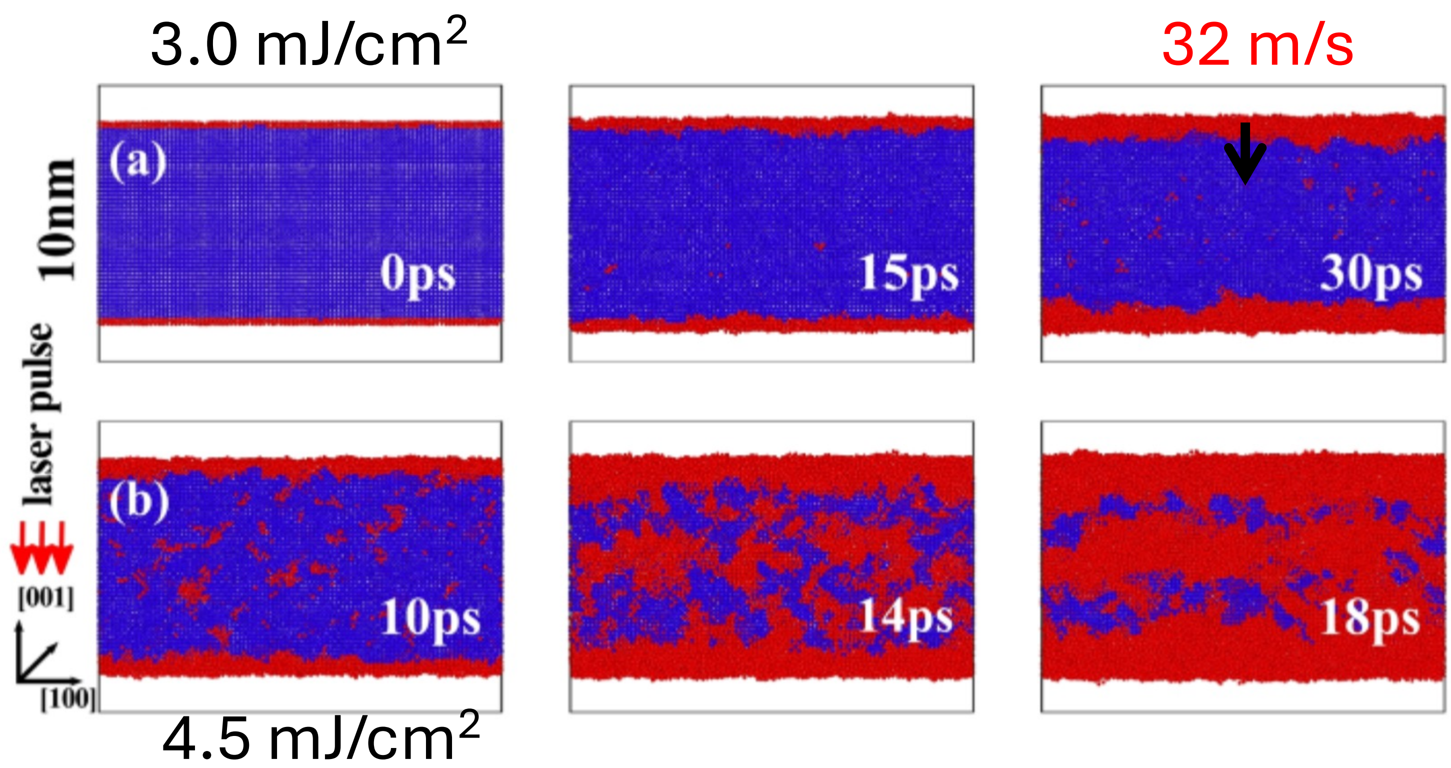

Grain Boundary Melting

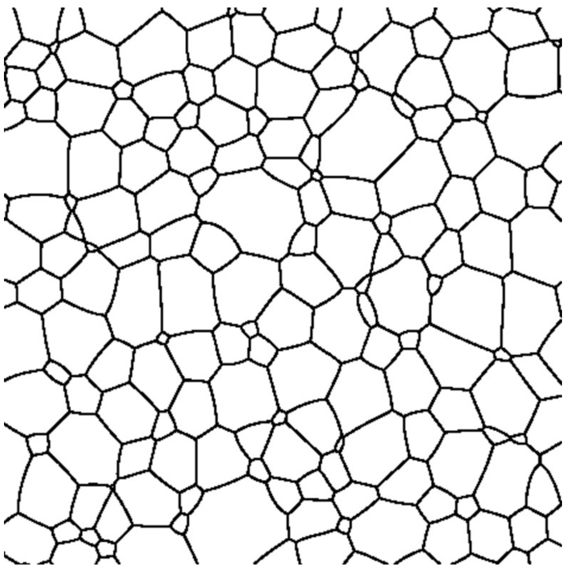

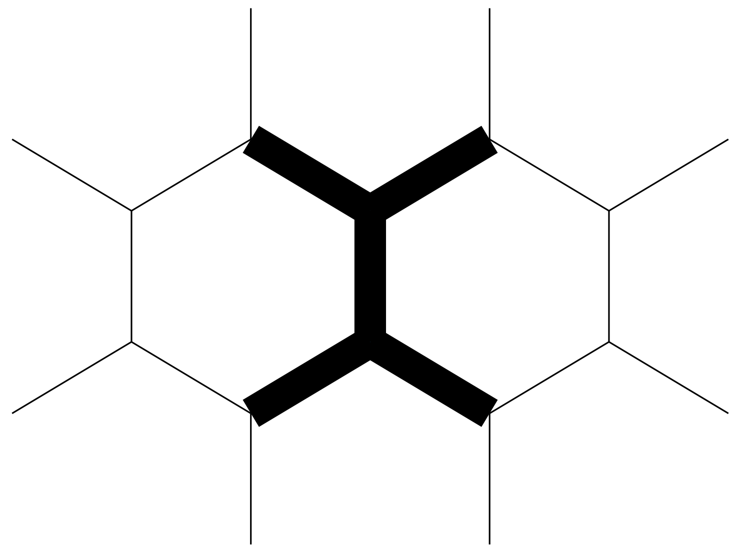

Grain Boundary Melting

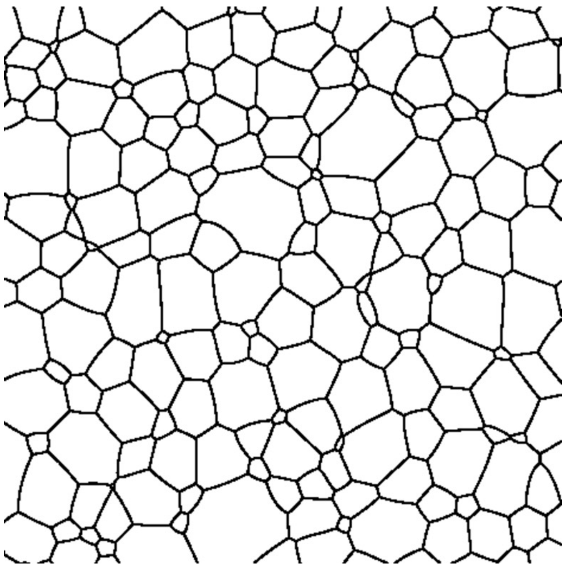

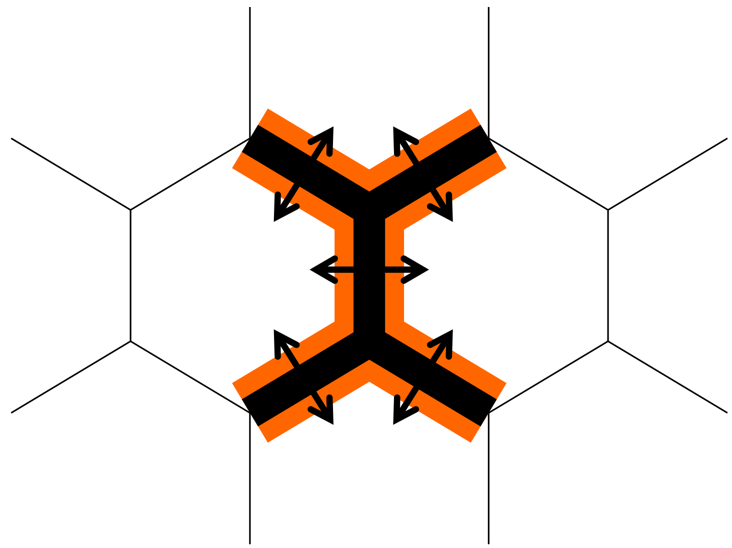

Force-Field Simulation of GB melting

J. Berry, K. Elder and M. Grant, PRB 77 224114 (2008)

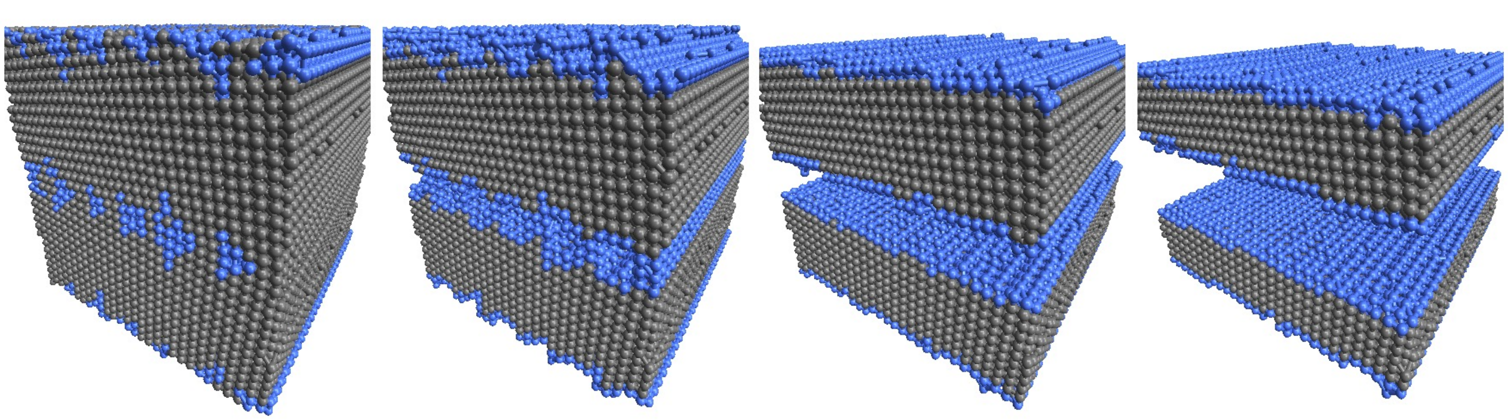

Grain Boundary Induced Melting

T. A. Assefa et al Science Advances 6 eaax2445 (2020)

$$K_o(\zeta,\tau)=\left(\frac{1}{4\pi D\tau}\right)^{1/2} e^{-\frac{\zeta^2}{4D\tau}}$$

$$\zeta = x - x' \qquad \tau = t - t'$$

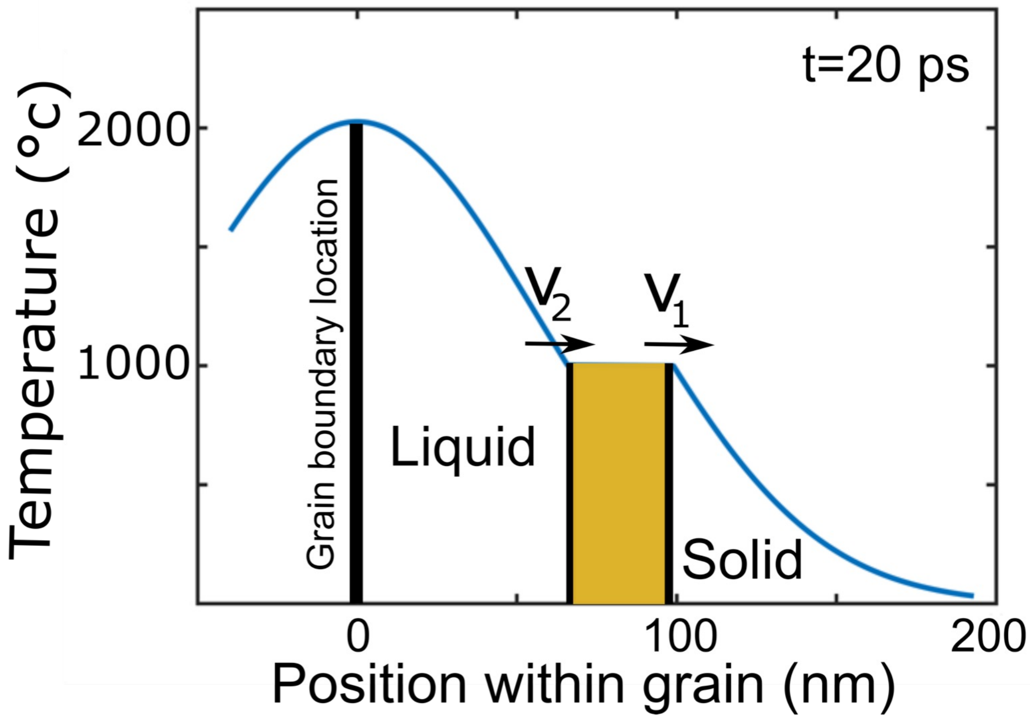

Deconvolution of Peaks

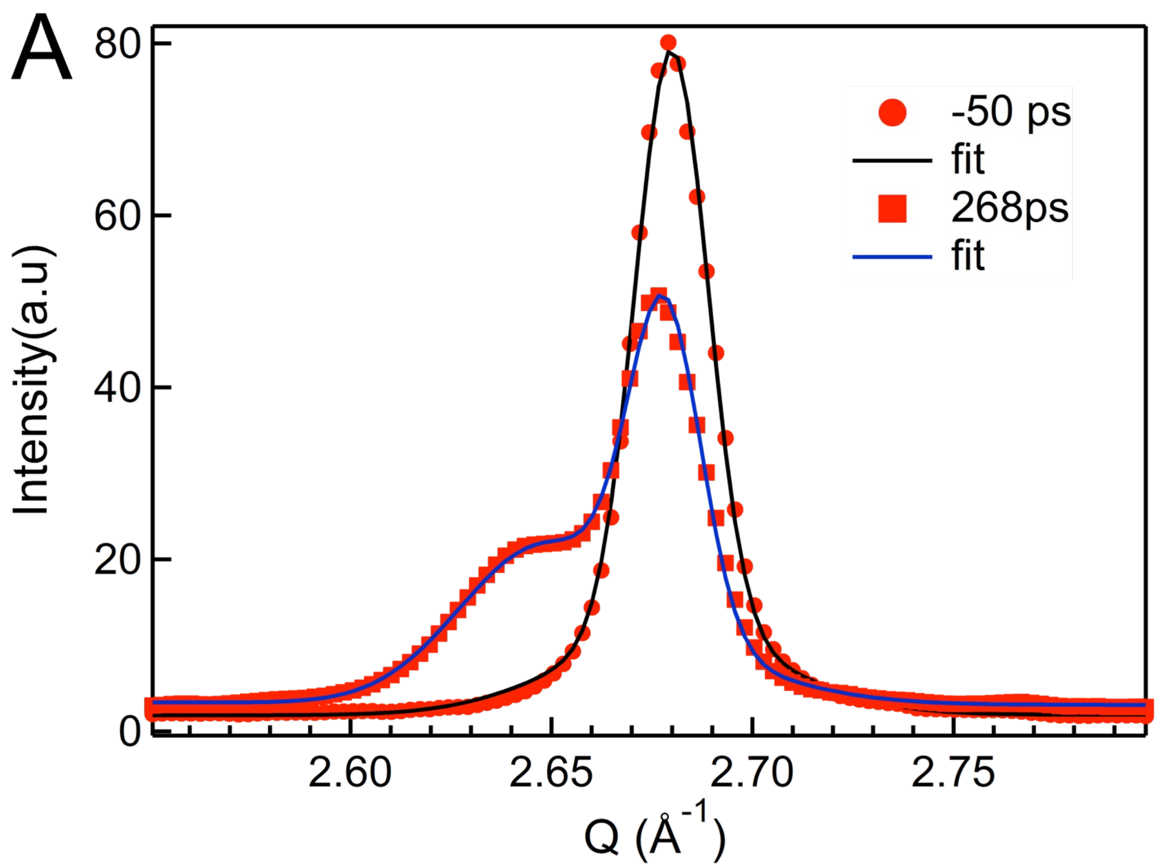

Pump-Probe kinetics of Crystal Peak

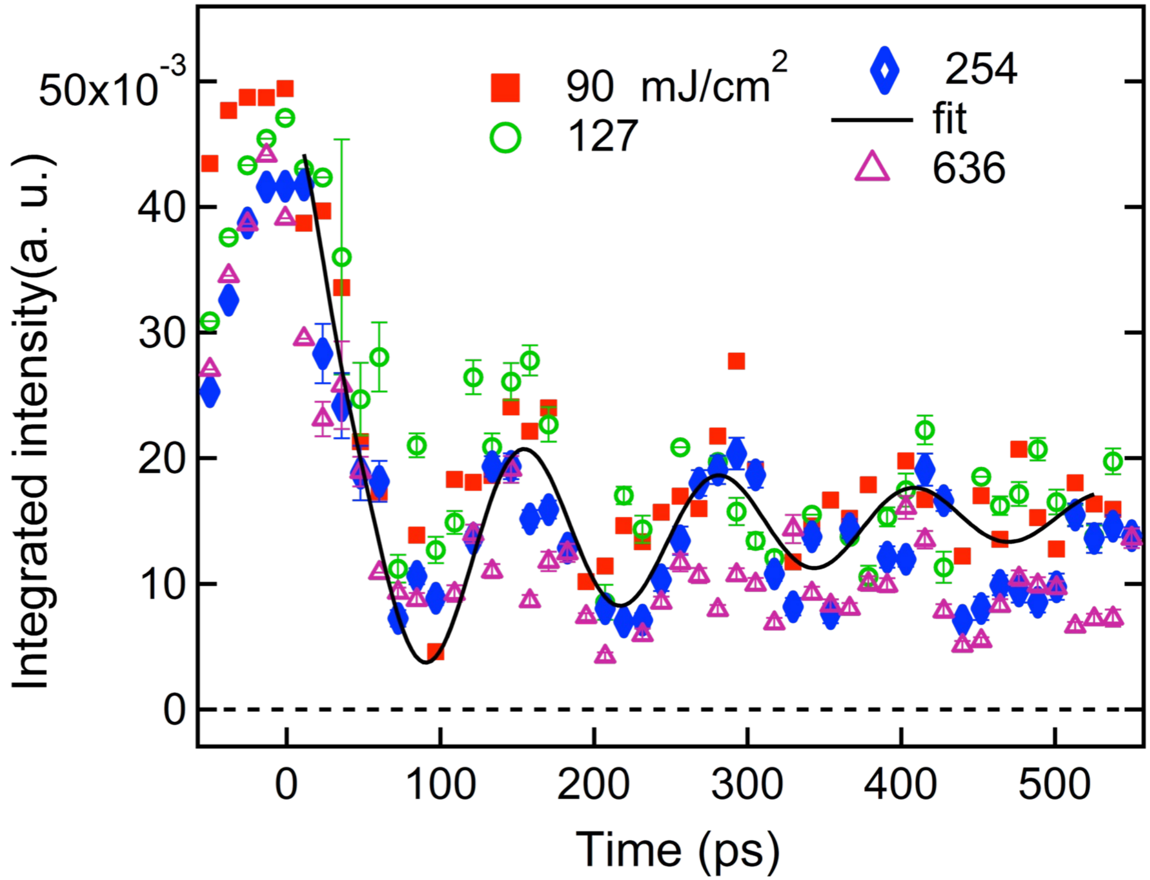

Width of Melt-Front Peak

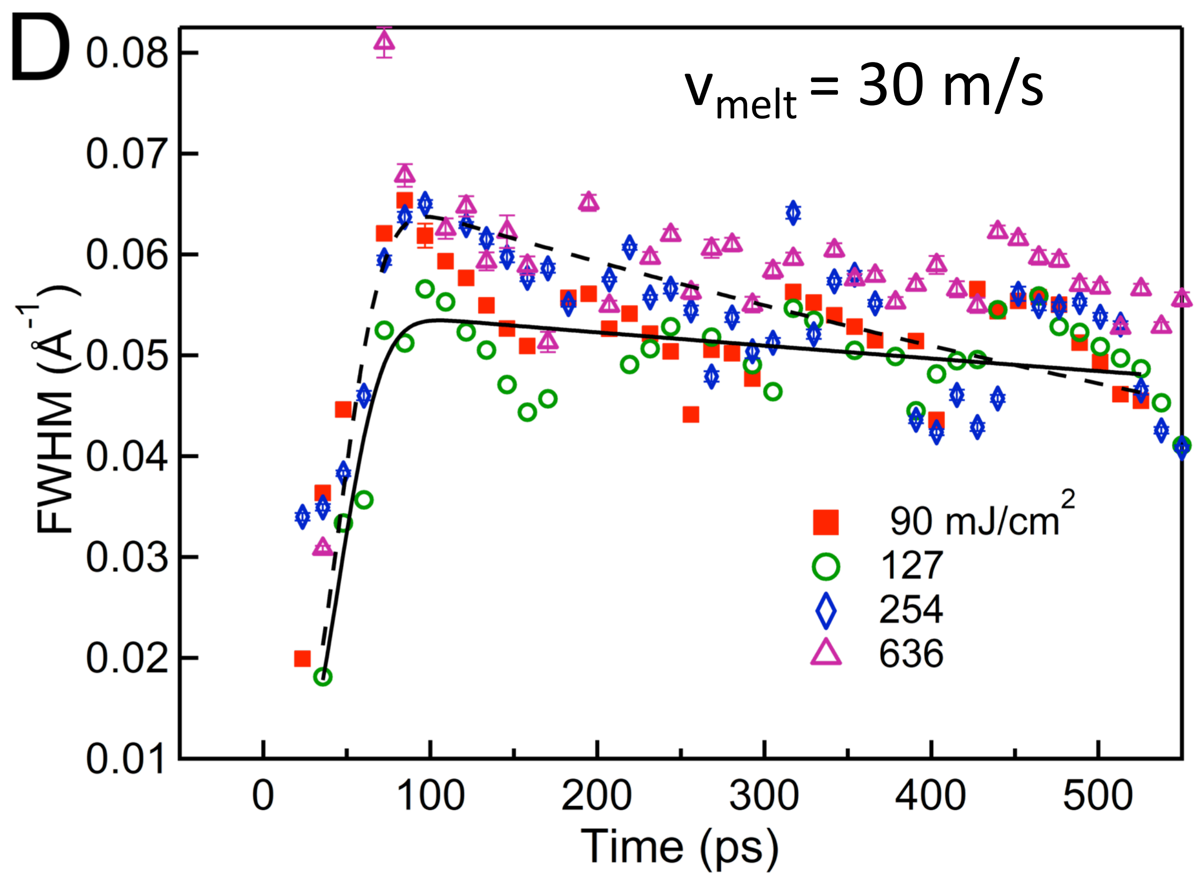

Palladium is Different from Gold

A. F. Suzana, et al, Phys. Rev. B 107 214303 (2023)

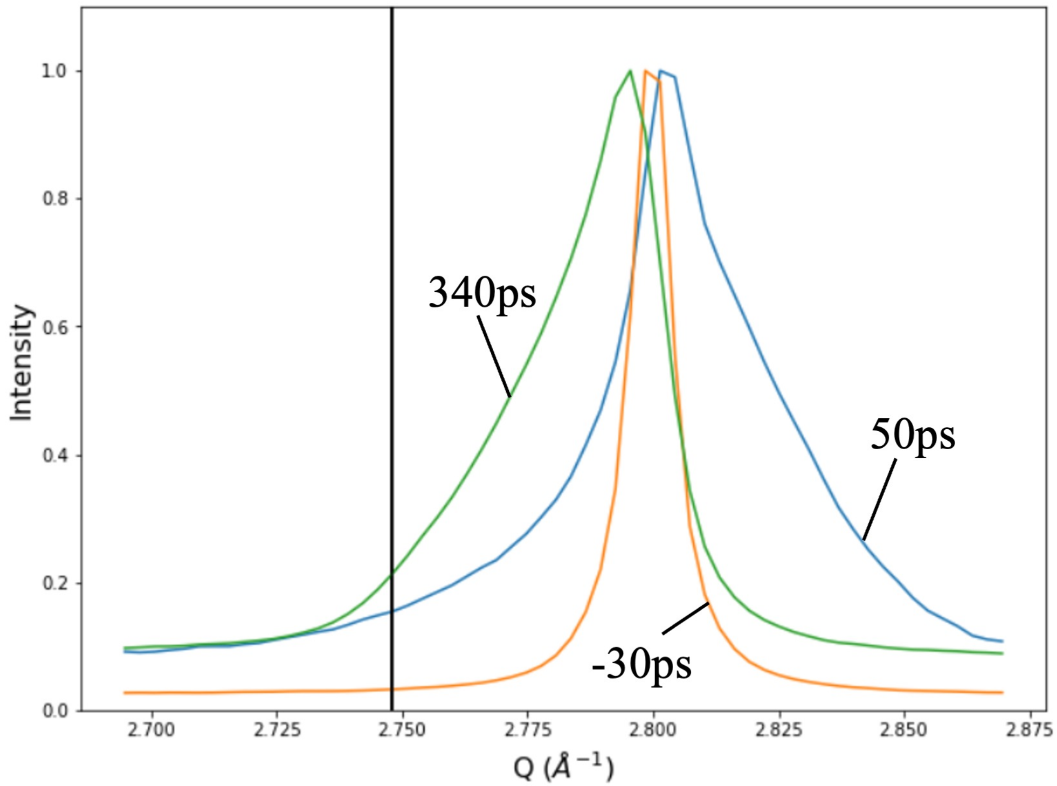

- (111) Bragg peak vs time delay
- 300 nm Pd poly thin film
- PAL XFEL
- laser fluence 800 mJ cm^{-2}

Nano Terasu directions 1

- 50nm films have SAXS features
- 400 nm grain size
- Changes after melting
- Possibly aniotropic
- Ptycho pre/post melt
- Extend to Cu films
- Laser machining …

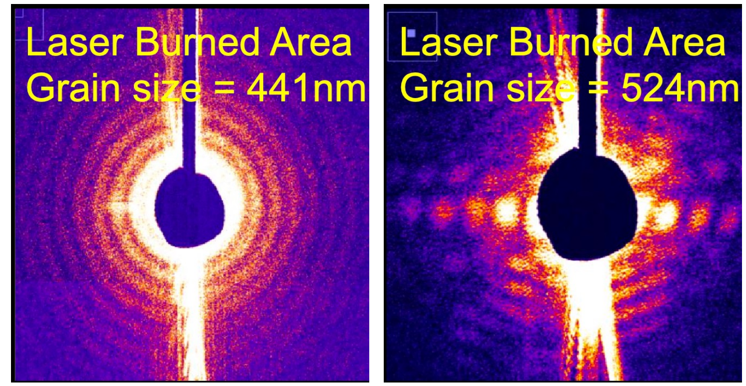

A. Plech et al, Nature Physics 2006

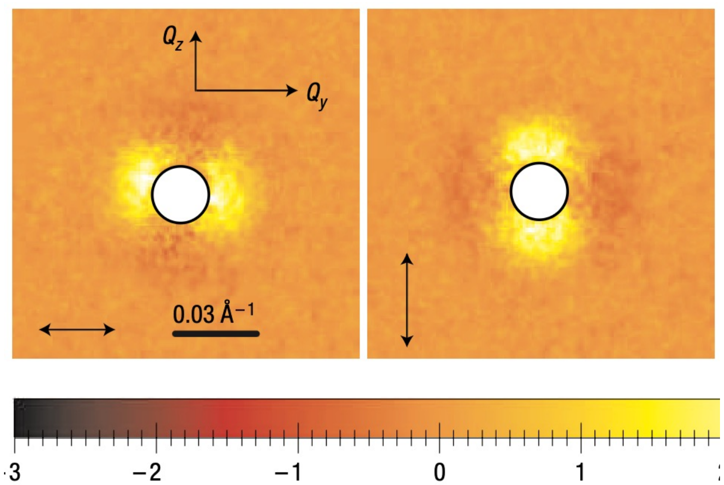

Laser Machining speed Comparison

50μm hole drilled in Alumina plate

Tatsuhiko Aizawa and Tadahiko Inohara, Book Chapter

“heat-affected zone”

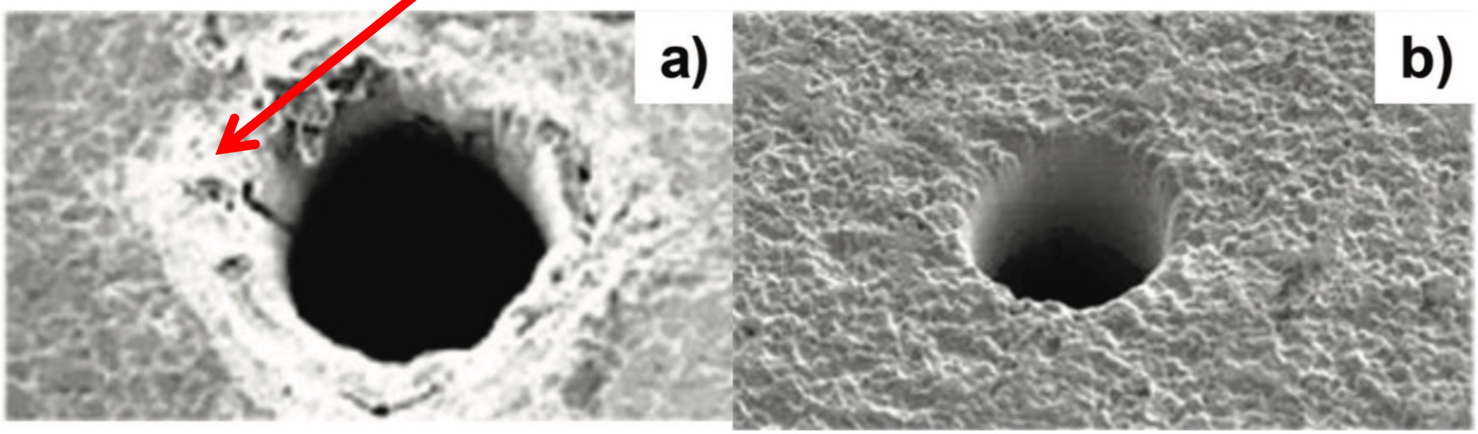

Figure 6.
Comparison of the drilled through-hole between fiber lasers and the picosecond laser. (a) Fiber laser drilling, and, (b) Picosecond laser drilling.

Nano Terasu directions 2

- Human chromosomes
- Compact in prophase “spread”
- Ptycho measures mass
- 46 chromosomes ranked
- Excess mass changes with damage
- Prof Fukui (Osaka)

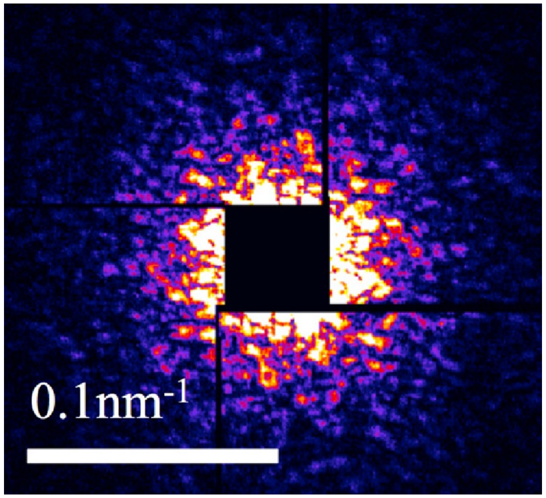

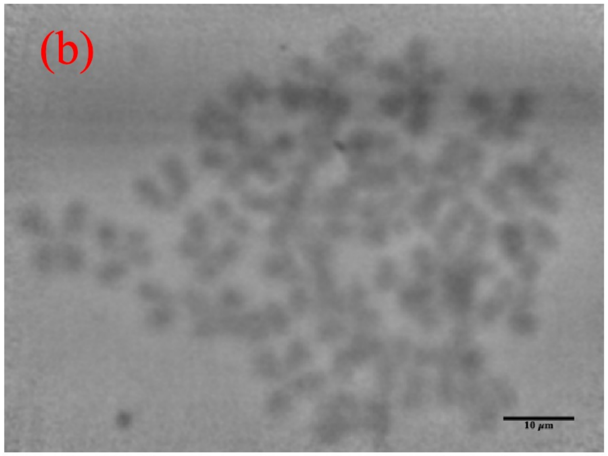

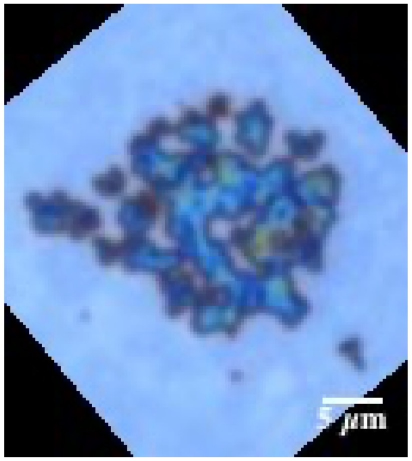

Nano Terasu directions 3
Energy dispersive Bragg Ptychography for thin films

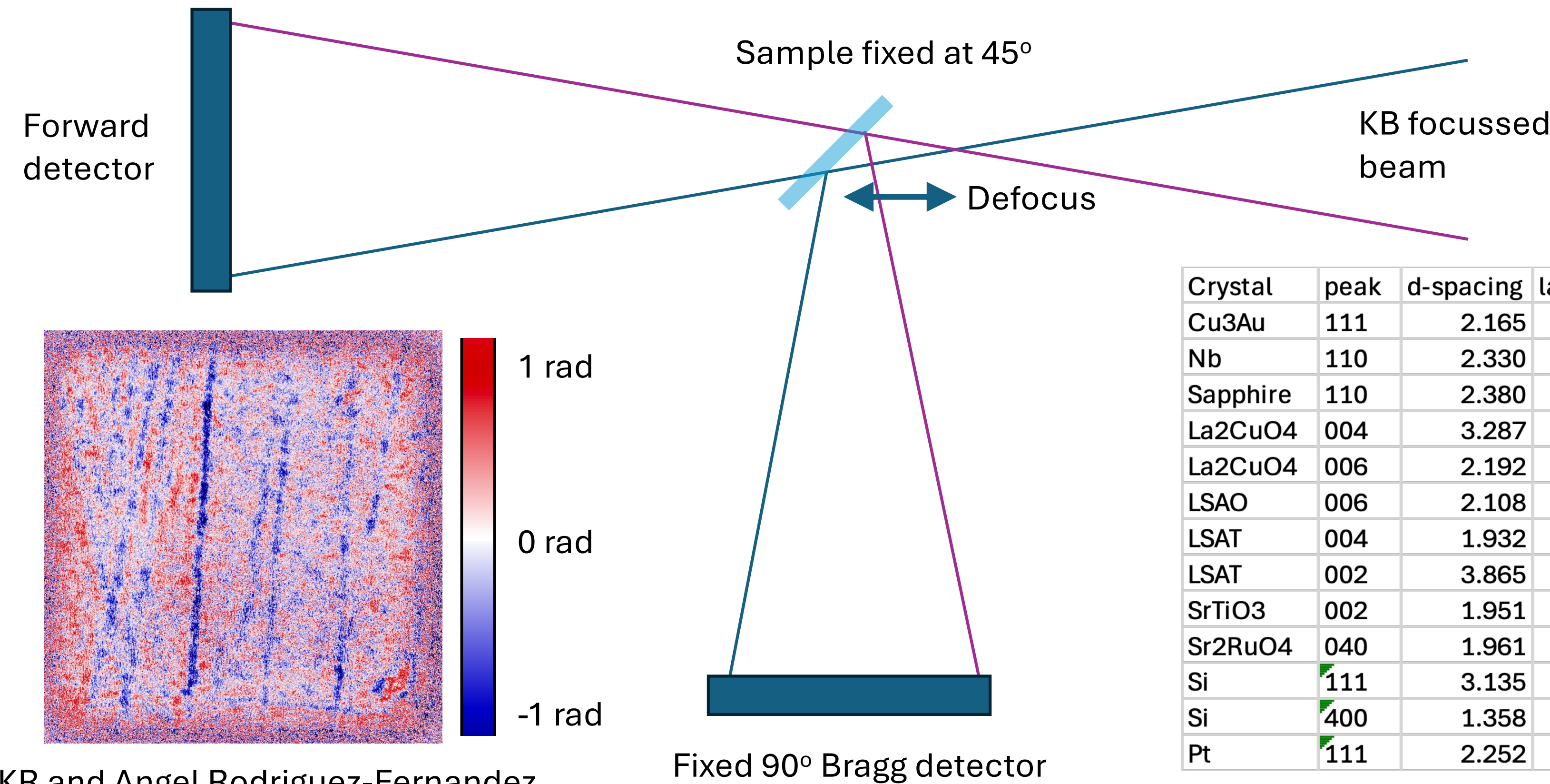

IKR and Angel Rodriguez-Fernandez, in preparation

Crystal	peak	d-spacing	lambda	energy
Cu3Au	111	2.165	3.062	4047
Nb	110	2.330	3.295	3760
Sapphire	110	2.380	3.365	3682
La2CuO4	004	3.287	4.649	2665
La2CuO4	006	2.192	3.100	3997
LSAO	006	2.108	2.981	4156
LSAT	004	1.932	2.732	4535
LSAT	002	3.865	5.466	2267
SrTiO3	002	1.951	2.759	4491
Sr2RuO4	040	1.961	2.773	4468
Si	111	3.135	4.434	2795
Si	400	1.358	1.920	6454
Pt	111	2.252	3.184	3891

Role of Phase Domains in Complex Materials

- Phase Domains
- Coherent Diffraction Imaging (CDI)
- Bragg ptychography
- Spin-ordered domains in $La_{2-x}Sr_xNiO_4$
- $BaTiO_3$ in Multilayer Capacitors
- Domains in solid state electrolyte crystals
- Possible connection with ball-milling
- Imaging role of domain walls in melting

Acknowledgements

Ruiyang Duan
Jialun Liu

David Yang
Longlong Wu
Ana Suzana
Tadesse Assefa
Yao Shen
Andi Barbour
Wei Wang
Claudio Mazzoli
John Tranquada
Mark Dean

Dongjin Kim
Sungwon Kim
Hyunjung Kim

Changyong Song
Heemin Lee

Yan Zeng
Bin Ouyang
Ajay Shaji

Sunam Kim,
Jae Hyuk Lee,
Yongsam Kim,
Jaeku Park,
Sang-Youn Park,
Intae Eom,
Hyojung Hyun,
Tae-Yeong Koo,
Jaehun Park,
Daewoong Nam
Sang Soo Kim

Fabian Westermeier
Wojciech Roseker

Dharma Prabhakaran
Andrew Boothroyd

Dina Sheyfer
Ross Harder
LuXi Li